LUND UNIVERSITY

Master of Science dissertation:

An investigation of a potential multi-purpose readout modality for two and three-dimensional dosimetry using optical computed tomography scanners

Henrik Svensson

Malmö, August 31, 2011

Supervisors:

Sofie Ceberg, Ph.D
Sven Bäck, Assoc. Prof

Clear eyes
Full hearts
Can't lose
    – motto of the Dillon Panthers

Abstract

Purpose: Radiochromic film, polymer gel and radiochromic plastic are three different kinds of dosimeters developed for radiation therapy. Even though all three types of dosimeters are suitable for optical scanning, the proposed readout method is different for each detector system. In this study, the scanning properties of three optical CT scanners were investigated to determine if they could be developed into multi-purpose scanners, i.e. be used for readout of more than one type of dosimeter.

Material and methods: The scanners used were the parallel beam CCD scanner and the fast laser scanner of the University of Surrey, UK and the Octopus IQ scanner located in Aarhus University, Denmark. Gafchromic EBT2 radiochromic films were cut into pieces and irradiated with calibration, conventional and advanced fields. Scanning was done on the parallel beam and Octopus IQ scanner and on a standard document flatbed scanner as reference. An nPAG polymer gel dosimeter was irradiated with a simple four-field box and then scanned with the Octopus scanner and MRI. To test radiochromic plastics, a Presage sample was irradiated and read out using the scanners from the University of Surrey and an identical RapidArc rotational beam field was irradiated on a polymer gel dosimeter and read out using MRI.

Results and discussion: The parallel beam EBT2 film evaluation using the flat panel approach gave similar results compared with the flatbed scanner results. The films read out using the Octopus scanner showed potential, but the method needs development to achieve images comparable to the ones from the flatbed scanner. The polymer gel readout of the Octopus scanner was comparable to the readout from MRI and TPS. The Presage readouts were subordinate to the gel readout with MRI for the same field. To be comparable to the MRI readout, better alignment and a Presage sample manufactured closer in time to the measurement is needed.

Conclusions: None of the scanners could be labeled a pure multi-purpose scanner today. However, all scanners show potential and with some further development it is possible that all scanners could be categorized as multi-purpose scanners. This would result in a very useful clinical QA tool.

Jakten på den perfekta scannern

Under det senaste decenniet har avancerade strålbehandlingsmetoder utvecklats i en allt snabbare takt. Dessa nya metoder syftar till att ge tumörområdet den ordinerade stråldosen samtidigt som organ runtomkring bestrålas med en så liten stråldos som möjligt. Detta innebär att risken för potentiella biverkningar minskar utan att det gör avkall på cancerbekämpningen. Tyvärr har inte utvecklingen av detektorsystem följt med i samma takt, vilket har lett till att vi nu har tekniker som enligt datorprogram bestrålar med fantastiskt resultat, men som är svåra att verifiera i verkligheten.

Tre detektorer som kan användas för att verifiera så att den givna stråldosen verkligen är vad den borde vara är radiokromisk film, polymergel och radiokromisk plast. Gemensamt för dessa tre är att de är genomskinliga och ändrar färg beroende på hur mycket de blivit bestrålade. Vanligtvis läser man ut dessa dosimetrar på olika sätt; radiokromisk film främst med fotoscanner, polymergel främst med MR-kamera och radiokromisk plast med optisk CT.

En optisk CT är en sorts skiktröntgenapparat som använder synligt ljus istället för röntgenstrålning. Den kan vara uppbyggd på flera olika sätt, men grunden är att ett objekt fästs i en rotationsmotor och ljus sänds in i objektet. På andra sidan objektet finns en detektor som registrerar intensiteten i ljuset i varje punkt och genom att rotera objektet och mäta intensiteten i många olika projektioner kan man med datorns hjälp få fram en tvärsnittsbild av objektet. Om objektet är en dosimeter som blivit mörkare eller mindre genomskinlig av strålning kan man på så sätt få fram tredimensionella volymer på fördelningen av stråldosen.

I detta projekt undersöktes möjligheter för att använda en optisk CT för alla tre dosimetrar. Det finns en rad fördelar för att utveckla en sådan produkt, bland annat skulle det bli billigt för institutionen som skulle vilja använda flera sorters dosimetrar och det skulle också bli behändigt för personalen som bara skulle behöva lära sig en maskin.

Tre olika optiska CT användes och vidareutvecklades, två belägna vid Surreys universitet i Storbritannien och en vid Aarhus universitet i Danmark. Olika test utformades och metoder togs fram för att undersöka potentialen hos de olika scannrarna. För att undersöka kvaliteten hos scannrarna jämfördes resultatet både mot dosplaneringssystemets egna uträkningar och referenser i form av scannade filmer från en fotoscanner och polymergel scannade med MRI.

Alla scannrar visade sig ge lovande resultat, men mer arbete måste till för att slutligen komma fram till den ultimata optiska scannern för de tre typerna av dosimetrar. Skulle detta lyckas har vi ett väldigt användbart verktyg vid framtida kvalitetssäkringsmätningar.

Abbreviations & Acronyms

2D	Two-dimensional
3D	Three-dimensional
ART	Algebraic Reconstruction Technique
AAA	Analytic Anisotropic Algorithm
AAm	Acrylamide
Bis	N,N'-methylene-bis-acrylamide
CCD	Charge-Coupled Device
CMOS	Complementary Metal–Oxide–Semiconductor
CT	Computed Tomography
FOV	Field Of View
IMRT	Intensity Modulated Radiation Therapy
LED	Light-Emitting Diode
MRI	Magnetic Resonance Imaging
NMR	Nuclear Magnetic Resonance
nPAG	Normoxic Polyacrylamide Gel
PC	Personal Computer
OD	Optical Density
QA	Quality Assurance
RCF	Radiochromic Film
SSD	Source-Skin Distance
THP	Tetrakis(hydroxmethyl)phosphonium
TPS	Treatment Planning System
VMAT	Volumetric Modulated Arc Therapy
VOI	Volume Of Interest

1. Introduction

More than 50 000 new cases of cancer are annually reported in Sweden and the number of people diagnosed have increased steadily during the last two decades (The Swedish Cancer Society, 2011). Cancer is the most frequent cause of death for people between the age of 15 to 75, but due to the development of more effective treatment methods and progress in research the prognosis of a cancer diagnosis have been significantly improved during the last decades (The Swedish Cancer Society, 2011).

Roughly 50% of all the patients treated for cancer will undergo radiotherapy, both as the only treatment method and together with surgery and chemotherapy. Over the years, external radiotherapy has developed into more sophisticated and complex techniques. These new techniques aims to reduce the treatment time and minimize the absorbed dose to surrounding healthy tissue, without affecting the coverage of the prescribed target. To do this, the novel techniques often utilize moving beams, small fields and steep dose gradients (Ceberg, 2010). Unfortunately, the dosimetry verification methods have not developed in the same pace as the treatment techniques, which means that failure in some aspect of the treatment might not be discovered using current detector systems and that could put the therapeutic effectiveness at a risk. To secure the treatment the dosimetric verification should ideally be done in 3D and preferably with high resolution.

Radiochromic film (RCF) is an independent 2D detector with high resolution. It has an active layer which, once irradiated, changes color and could be calibrated to absorbed dose (International Speciality Products, 2009). RCFs are no 3D dosimeters per se, but might simulate 3D if stacked and could be used to verify fields at a certain depth (Devic, 2011). Polymer gel dosimeters are a promising group of pure 3D dosimeters, often a hydrogel containing monomers (Baldock *et al.*, 2010). Irradiation initiates free radical polymerization reactions from the monomers in proportion to the delivered dose (Baldock *et al.*, 2010). Another pure 3D dosimeter is Presage (Heuris Pharma LLC, NJ, USA), a solid and optically clear dosimeter made of polyurethane and a leuco dye that changes color when irradiated (Adamovics *et al.*, 2006). Common to all three types of dosimeters is that they are all suitable for optical readout.

The primary objective of the research reported in this thesis was to explore the possibility and potentially develop a method of using an optical CT scanner as a multi-purpose device for readout of all three dosimeter types described. The RCFs are often read out using a standard commercial flatbed scanner, but these are not primarily designed for measuring RCFs. Polymer gel dosimeters could both be read out optically and with MRI, but for many institutions the

access to an MRI scanner is limited, which makes gel readout both costly and cumbersome. Since an optical CT scanner is much cheaper than an MRI unit, it could be a valid option for institutions that wishes to conduct research with polymer gel dosimeters and want to do it independent from the clinic. In modern scanners, the readout of gels is generally much faster for an optical CT than for MRI and, furthermore, optical CT scanning is the only viable readout option for Presage. Since the emission spectrum of the optical CT scanners, that are designed for readout of radiochromic plastics and gels, overlaps the absorption peak in Gafchromic EBT2 (the most common RCF in radiotherapy), the scanners are potentially convenient and economical for both film and 3D dosimetry (Babic *et al.*, 2010).

The optical CT scanners used in this work were a parallel beam CCD scanner (Krstajic *et al.*, 2006; Krstajic *et al.*, 2007a) and a fast laser scanner (Krstajic *et al.*, 2007b; Krstajic *et al.*, 2009) from the University of Surrey, UK, and the commercial laser scanner Octopus IQ (MGS Research, Inc., Madison, CT, USA) located in Aarhus, Denmark.

In order to evaluate the potential of the optical CT devices for multi-purpose scanning, following specific aims were established:

- ❖ To investigate RCFs irradiated with different fields and compare readouts with optical CT scanners to readouts with a commercial flatbed scanner
- ❖ To investigate a polymer gel dosimeter readout with an optical CT scanner versus MRI.
- ❖ To investigate the two 3D dosimetry systems; Presage using optical CT scanner and polymer gel using MRI.

2. Background

Since this study aims to investigate different optical CT's, an explanation of the basic idea behind the device and the state of the optical CT today are presented below.

2.1 Optical CT

An optical CT scanner uses a technique that in many ways are analogous to the first generation x-ray CT, except for the visible light source that is used instead of an x-ray source (Oldham, 2004). Another mentionable difference is that the sample rotates instead of the source.

Beer-Lambert's (or Beer's) law is the starting point to all work in optical CT and it describes how photons are attenuated as they pass through a medium (Krstajic *et al.*, 2007a). For an absorbing medium, Beer's law will hold down to a high degree of opaqueness, while it will break down much earlier for a scattering medium (Doran, 2009b). The optical absorbance of photons with wavelength λ is calculated by

$$A_\lambda = \log_{10} \frac{I_0}{I} \tag{1}$$

where I is the intensity of the light detected that has passed through the sample (transmitted irradiance) and I_0 the intensity of the light detected without the sample (incident irradiance) (Krstajic *et al.*, 2007a).

One definition of optical density is the absorbance per unit distance of the material traversed. This means that OD is an intensive property and may have different value at every point, r. For a certain light path through the sample, OD has the following relation to absorbance:

$$A_\lambda = - \int_{ray\ path} OD_\lambda(r)\mathrm{d}l \tag{2}$$

where l is the distance of the ray-path through the sample (Krstajic *et al.*, 2007a). This definition means that OD_λ has units of inverse distance (e.g. cm^{-1}) and could be said to be the analogue to the monochromatic linear attenuation coefficient in x-ray CT. If optical projections are obtained when the sample is positioned in different angles, it is then possible to mathematically reconstruct 3D images of OD_λ. In optics, the term optical density could also be used as a synonym for the absorbance and is then unit-less.

To avoid artifacts related to differences in refractive index between the dosimeter, the container wall (for the polymer gel dosimeter) and the surrounding air, the sample is positioned in a square bath that contains an index-matched liquid (Baldock *et al.*, 2010). Another improvement that can be done is the addition of a dye to the matching liquid. The dye should give the liquid similar absorption properties as the sample and the dynamic range of the detector would then be used most efficient.

2.1.1 Brief history

A description of a prototype optical CT scanner made for 3D dosimetry was published in 1996 (Gore *et al.*, 1996). The sketch presented there is shown in figure 1. In this setup, a laser beam steps across a sample by mechanically moving two synchronous mirrors and the resulting beam is measured using a photodiode detector. The scanner was eventually developed into the first commercially available optical CT system, the Octopus scanner from MGS Research, Inc. and that scanner is currently regarded as the first generation and the origin of all optical CT scanners for 3D dosimetry (Doran, 2009b; Doran, 2009a).
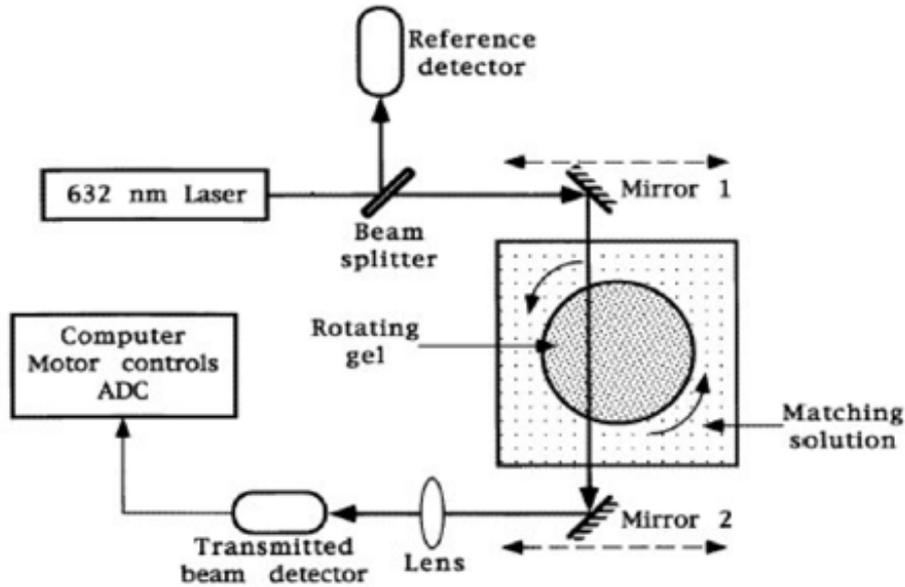
Figure 1: A sketch showing the prototype optical CT for 3D dosimetry (Gore *et al.*, 1996)

The first generation scanners suffered from slow scanning speed due to the mechanical movement of the mirrors. A single slice with 128 x 128 pixels were acquired in about 12 minutes (Doran, 2009b). However, due to their precise measurements, the first generation scanners have been referred to as the "gold standard" of optical CT scanners (Doran, 2009b). Two major branches of optical CT systems have since then been developed and together they could be considered as the second generation of optical CT scanners. Those are the pixelated area detectors and the fast laser scanners (Doran, 2009b).

2.1.2 Pixelated area detectors

The pixelated detectors are based on either CCD or CMOS chips and are able to obtain a whole 2D projection instantly at each rotation step, which render a significant speed advantage (Doran, 2009a). The speed and resolution of this type of scanner is superior, but the sensitivity to refractive index inhomogeneities and stray photons from the dosimeter and the walls surrounding it can be a problem when the absorbed dose is reconstructed into a 3D map. The reason for this is that the entire projection is formed from one single exposure of the entire dosimeter (Doran, 2009b). Today, this type of scanner is divided into two different sub-classes with different geometries; the cone-beam and the parallel beam (Doran, 2009b).

Cone-beam geometry

Since the first cone-beam geometry presentation (Wolodzko *et al.*, 1999) it has been used in a number of devices worldwide, for example in the commercial scanner Vista (Modus Medical Devices, London, Canada). Due to the familiar geometry of a clinical cone-beam CT, various promising scatter correction methods have been applied to counter the scatter issues in pixelated

4

area detectors (Jordan *et al.*, 2009; Olding *et al.*, 2009; Olding *et al.*, 2010). The basic principles of a cone beam optical CT is illustrated in figure 2 and a photo of the Vista scanner is showed in figure 3. No scanner using the cone-beam geometry was used in this thesis.
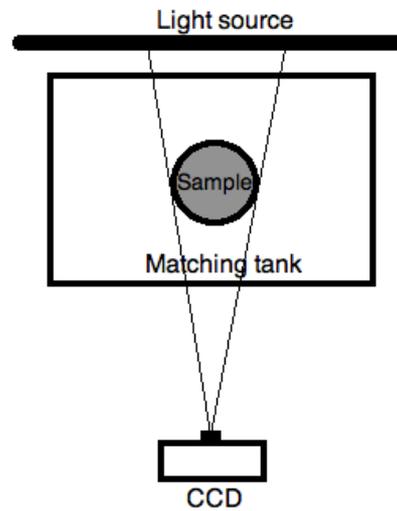
Figure 2: An optical CT with the cone-beam geometry

Figure 3: The commercial Vista scanner (www.modusmed.com). The dimensions of the region of interest is up to 15 cm diameter and 12 cm long for the largest Vista scanner available

Parallel beam geometry

The scanners based on the parallel beam geometry use telecentric optics to create beams that travel parallel through the sample and are focused on the detector (Doran, 2009b). The configuration is used in one of the scanners at the University of Surrey that is examined in this thesis. The basic principles of the parallel beam geometry are illustrated in figure 4.

Figure 4: An optical CT with the parallel beam geometry

2.1.3 Fast laser scanners

The fast laser scanners are the result of trying to modify the design of the first generation scanners by getting rid of the time consuming mechanical translation of the beam (Baldock *et al.*, 2010). The movement of the laser beam rapidly through the sample studied is done either by rotating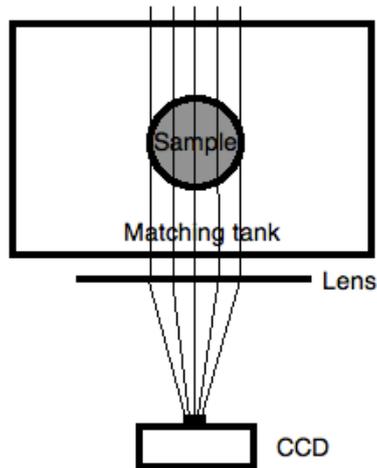 mirrors or galvanometer mirrors. Since the beam has to be moved through the sample in each slice, the scanning time is often longer than for pixelated area detectors (Doran, 2009a). Because only one path through the sample is measured at a time, the laser scanners are free from scattering artifacts and the signal-to-noise ratio is superior due to the high intensity of the laser beam. However, the rapid movement of the beam requires more complex optics that could lead to artifacts or distorted images, which needs more post-processing.

An example of a scanner using rotating mirrors is an evolved version of the original Octopus scanner, called Octopus IQ (Zeidan *et al.*, 2010), while the fast laser scanner from the University of Surrey is based on the galvanometer approach (Krstajic *et al.*, 2007b).

2.2 Fundamental optics

2.2.1 Telecentric optics and parallel beams

A lens forming an image can be seen as the focusing of a bunch of rays, or a cone, radiating from each point of the depicted object (Krstajic *et al.*, 2006). The ray in the center of the cone is called the chief ray and the rays along the edges of the cone are called marginal rays. For an optical system to be defined telecentric, the chief rays should be parallel in object space (Krstajic *et al.*, 2006). In optical CT scanners, a telecentric geometry could be arranged between two plano-convex lenses; the first having a point source in its object space focal point, thus making the chief rays parallel in its image space. The second focus these parallel rays either on a CCD lens or a photoreceiver, depending on scanner type. Alternatively Fresnel lenses could replace the plano-

convex lenses. The two lens-combo is used to ensure that the beam that goes through the sample, situated between the lenses, are parallel and creates images suitable for tomography reconstruction (Krstajic *et al.*, 2006). Telecentric geometry is also used to reject stray light, since the rays that do not travel parallel into the second lens will be rejected by the optics, i.e. they will not be focused on the detector. This means that light rays that travel in paths that are parallel to the optical axis will dominate the image formation (Krstajic *et al.*, 2006).

3. Material and methods

In this study, three different dosimeters were scanned with various readout modalities. Section 3.1 covers the different scanners and section 3.2 the dosimeters used. As the focus was to investigate the optical CT scanners, they are described more extensively than the other modalities. Readout methodologies are presented in section 3.3, 3.4 and 3.5. New methods were also developed, as described in section 3.1.3 and 3.3.3.

3.1 Readout modalities

3.1.1 Epson Perfection 4990 Photo flatbed scanner

Commercially available flatbed scanners are the recommended digitizing method for the radiochromic Gafchromic EBT2 film (ISP corporation, NJ, USA) (International Speciality Products, 2009). A flatbed scanner usually has a glass pane, a bright light and a CCD array that is moved during the scanning. Epson Perfection 4990 Photo (Seiko Epson Corp., Nagano, Japan) was used for readout of films in this thesis. This scanner model has been shown to be a good modality for the task of scanning RCFs (Sakhalkar *et al.*, 2009; Stunja *et al.*, 2010). An image of the scanner can be seen in figure 5.

Figure 5: Epson Perfection 4990 Photo flatbed scanner (www.epson.se)

3.1.2 Parallel beam CCD scanner in the University of Surrey

One of the optical-CT apparatus tested in this study uses the pixelated area detector approach. It is developed by scientists at the University of Surrey and has a CCD chip and the parallel beam geometry earlier described in section 2.1.2 (Krstajic *et al.*, 2006; Krstajic *et al.*, 2007a).

A schematic top view of the scanner containing a 3D dosimeter is given in figure 6 and the setup is shown in figure 7. The red LED light source (LedR – BL -20 mm x 20 mm – LLUB – Q – 1R – 24V, 633 nm, Phlox Corp., Aix en Provence, France) is placed behind a pinhole collimator,

which assure a point-like light source. The pinhole is placed in the focal point of the collimating plano-convex lens L1 (01-LPX-336, 440 mm focal length, 145 mm diameter, Melles Griot, Irvine, CA, USA). When the light passes through L1, parallel beams are created and passes through the sample. The non-attenuated parallel beams passes through the next plano-convex lens, L2 (custom design, 500 mm focal length, Optical Surfaces, Kenley, UK), and are focused first onto the CCD lens and eventually onto the CCD chip of the camera (Orca 1024 BTII, part number C4742-98-26-KAG, Hamamatsu Photonics Kabushiki Kaisha, Shizuoka, Japan). The camera is connected to a PC where the projections are collected.
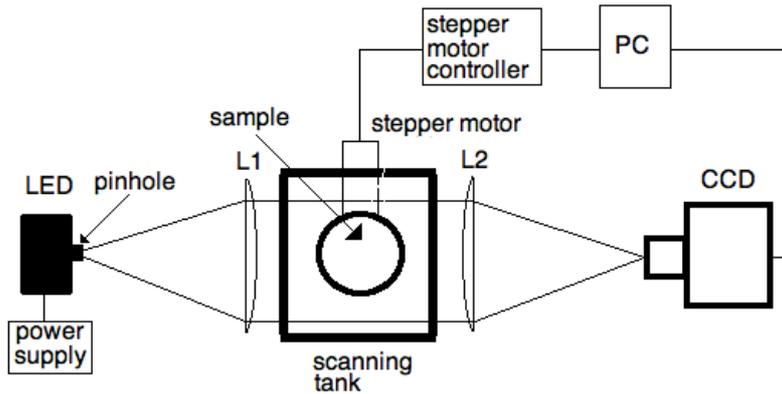
Figure 6: Schematic top view of the CCD scanner with a 3D dosimeter as the sample
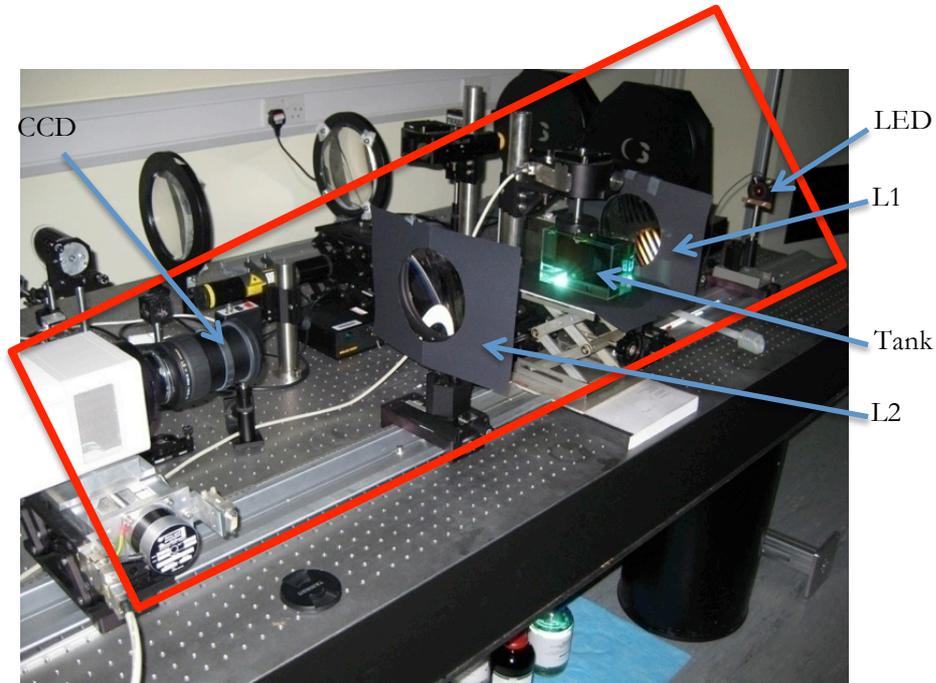
Figure 7: The CCD scanner described in the schematic in figure 6

To rotate the 3D dosimeter, the sample is positioned on a stepper motor driven rotation stage (PRS-110 ZSS43, Micos Gmbh, Eschbach, Germany) situated above the scanning tank and connected to the PC. The image acquisition is then performed with software written in Visual Basic (Microsoft Corp., Redmond, WA, USA) made by the creators of the scanner. The software

synchronizes the CCD image collection with the step motor rotation, controlled by a discontinuous step and shoot protocol.

After the image acquisition, the optical absorbance, $A(x, y)$, is calculated for each pixel in each projection of the dosimeter, $P(x, y)$ using

$$A(x,y) = \log_{10} \frac{L(x,y) - D(x,y)}{P(x,y) - D(x,y)} \qquad (3)$$

Equation (3) is derived from equation (1) in section 2.1. $L(x, y)$ is the light field, which is defined as the projection without the sample (dosimeter). $L(x, y)$ could also be obtained from the projection of an un-irradiated dosimeter. $D(x, y)$ is the dark field, which is defined as the projection without any light hitting the CCD chip. The reconstruction of the absorbance projections is carried out using constructed software in IDL 6.3 (ITT Visual Information Solutions, Boulder, Colorado, USA).

3.1.3 The flat panel approach of the CCD scanner in the University of Surrey

Telecentric optics and parallel beams might not be necessary when scanning 2D objects, since there is no tomography reconstruction to consider. Thus the CCD scanner described in section 3.1.2 was modified using a flat panel and tested with the Gafchromic EBT2 films. The flat panel system is shown as an illustrated top view in figure 8 and the setup is shown in figure 9. The framework holding the film is placed just in front of and parallel to a large LED screen (LedR - BL -100 mm x 100 mm – S – Q – 1R – 24V, 633 nm, Phlox Corp., Aix en Provence, France) that is big enough to illuminate the entire film. The CCD camera is focused on the film.
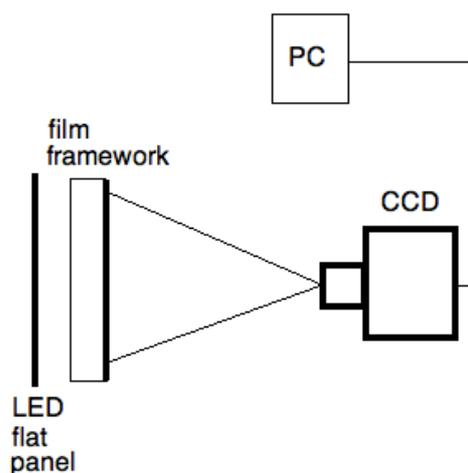
Figure 8: Schematic top view of the flat panel line-up
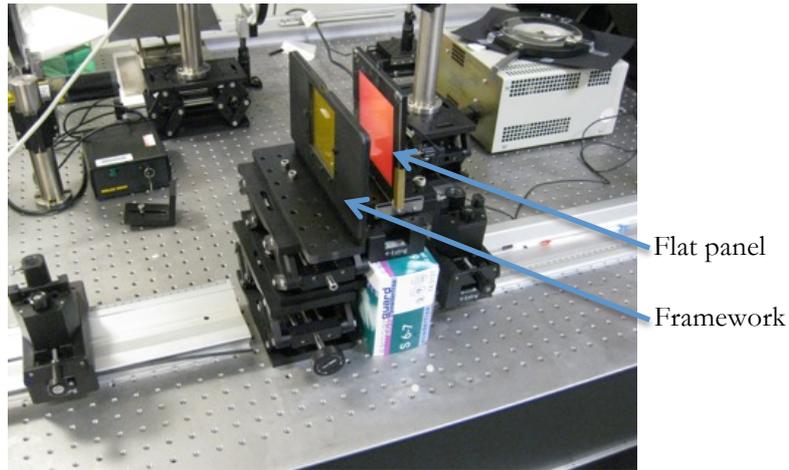
Figure 9: Experimental setup from figure 8. The CCD camera is located outside the image to the left

3.1.4 Fast laser scanner in the University of Surrey

One of the most sophisticated versions (Doran, 2009b) of the second-generation laser scanners was invented and built by researchers at the University of Surrey (Krstajic *et al.*, 2007b; Krstajic *et al.*, 2009).

The scanner uses galvanometer mirrors and relay optics to quickly scan the laser beam in a raster scan fashion with good repeatability and telecentric geometry to ensure that the laser beam path through the sample measures attenuation in a direction that is suitable for elementary tomography reconstruction, i.e. with parallel beams. The scanning arrangement utilizes concepts from the field of confocal microscopy (Pawley, 2006).
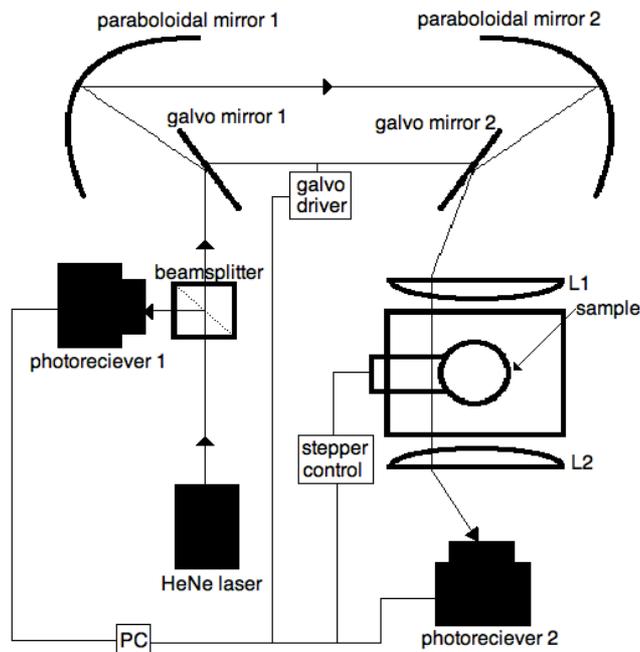
Figure 10: Schematic top view diagram of the fast laser scanner
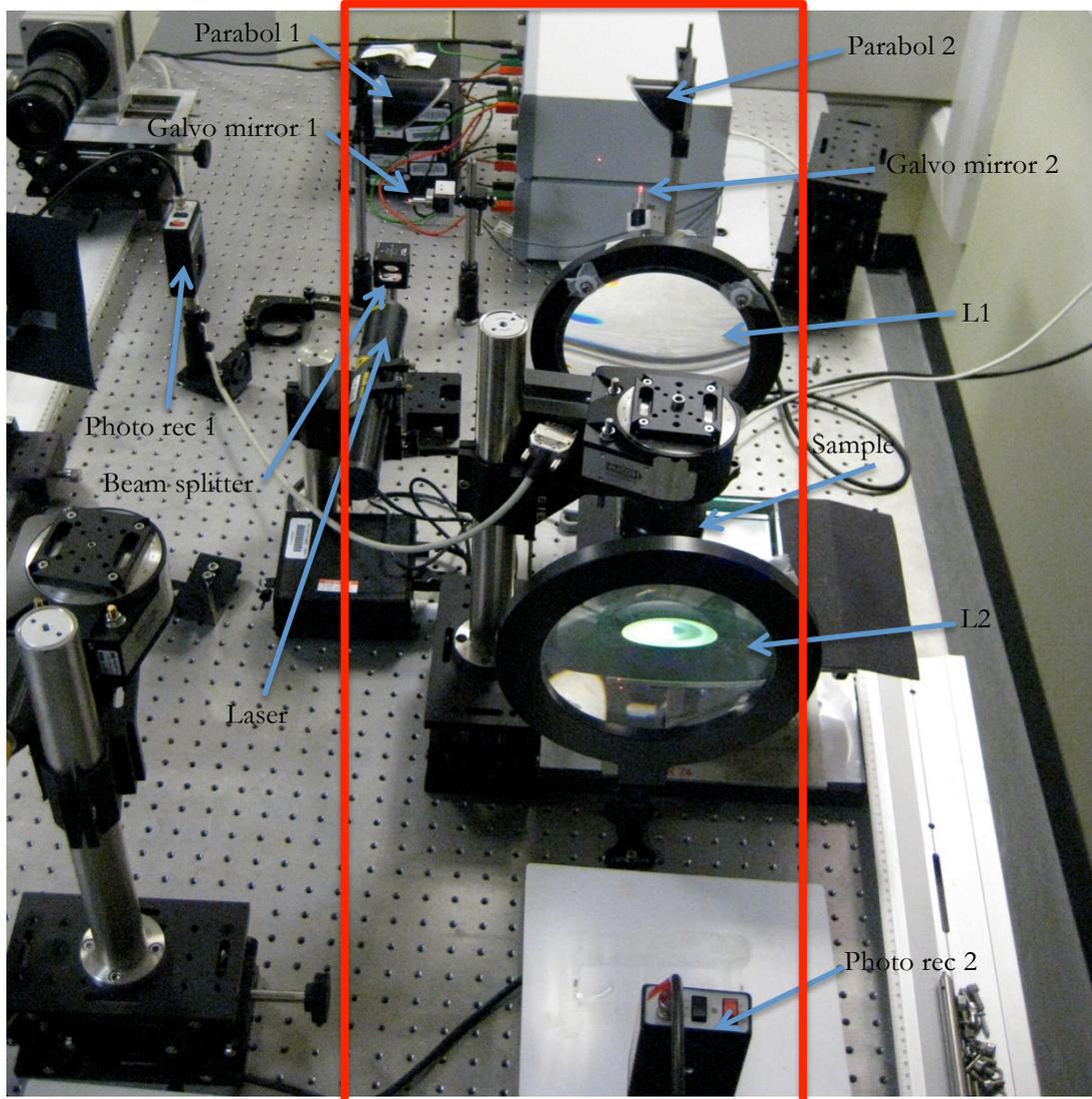
Figure 11: The fast laser scanner in the University of Surrey

A schematic diagram of the fast laser scanner is illustrated in figure 10 and the setup is showed in figure 11. The light source of the apparatus is a He-Ne laser (25-LHP-121-230, 2 mW, 0.59 mm beam width, 633 nm, Melles Griot, Irvine, CA, USA) that shines through a beam splitter with 50/50 ratio (CMI-BS1, Thorlabs, Newton, NJ, USA). One of the split beams is then read out by a photoreciever (8 mm diameter, model 2031, New Focus, Irvine, CA, USA) providing the light field value that is essential when determining attenuation. The other beam continues into the "relay optics", which consists of two galvanometer mirrors (QuantumScan5, Nutfield Technology Inc., Windham, NH, USA) and two off-axis paraboloidal mirrors (02 POA 017, Melles Griot, Irvine, CA, USA) (figure 12). This relay optics is an arrangement that was presented in a patent application (Amos, 1991) and was used in some obsolete Bio-Rad confocal microscopies (Pawley, 2006).

The main idea behind the arrangement is that the two galvanometers rotate on perpendicular axes, and provide movement in both the x- and y-axis (figure 12). The spot on which the laser is

pointed on the first of the galvanometer mirrors is at the focal point of the first paraboloidal mirror and after the beam is reflected there, it passes into both paraboloidal mirrors successively and is eventually reflected on a stationary pivot point on the second galvanometer mirror. The latter is situated in the focal point of the second paraboloidal mirror. Thus, the reason of having the two off-axis paraboloidal mirrors is to keep the beam on the second galvanometer mirror static even though the angle of the beam's reflection from the first galvanometer mirror changes with the galvanometer's movement. The pivot point on the second galvanometer mirror is situated in the focal point of the plano-convex lens L1 (01-LPX-336, 440 mm focal length, 145 mm diameter, Melles Griot, Irvine, CA, USA), making the beam exiting L1 into the dosimeter area parallel to the optical axis in a telecentric geometry. By sending appropriate waveforms to the galvanometer drive, the angle of the beam exiting the second galvanometer mirror is done in a way that the scanning is made in a rectangular raster fashion across the sample. The attenuated beam is finally focused from lens L2 (custom design, 500 mm focal length, Optical Surfaces, Kenley, UK) to the second photoreciever (8 mm diameter, model 2031, New Focus, Irvine, CA, USA).
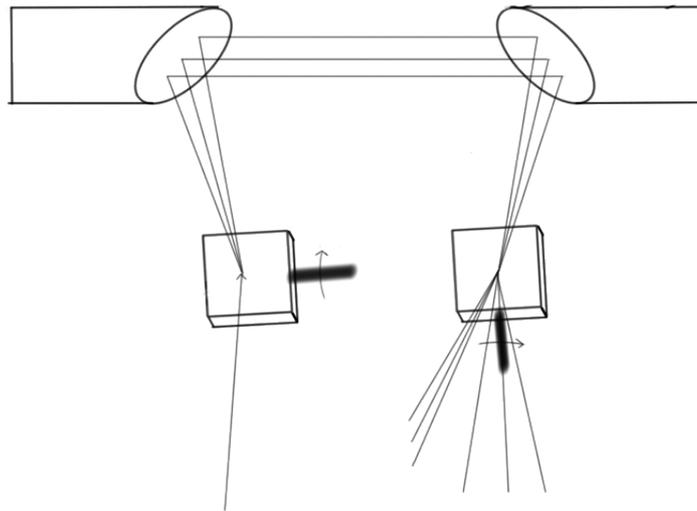
Figure 12: Schematic view showing the relay optics for the fast laser scanner

The signal is acquired synchronously in the two photoreceivers for each projection and the rotation stage (PRS-110, Micos Gmbh, Eschbach, Germany) rotates the sample after each projection. The whole process of sending waveforms to the galvanometer drive (QuantumDrive5000, Nutfield Technology Inc., Windham, NH, USA), data acquisition and sample rotation are controlled with an in-house written software in TestPoint (Capital Equipment, Keithley, Germering, Germany).

The data, i.e. the voltage, from the photoreciever can be used to compute optical absorbance according to equation (1) since the voltage is proportional to the irradiance of the laser beam. In equation (1), I_0 is the voltage measured in the beam from the first photoreciever and I from the

second. Thus, optical absorbance images can be obtained directly from the voltage ratios of the two photoreceivers.

Because of the setup arrangement of the scanner, the projections have to be corrected for distortion. This was carried out using the WARP_TRI algorithm in IDL 6.3. The algorithm uses pre-defined tie points from an original image of a sinusoidal test target (part NT54-803, Edmund Optics, Barrington, NJ, USA) and connects them to the same point in the corresponding distorted image of the target from the scanner. An image of the test target is shown in figure 13. Reconstruction of the absorbance projections is done using an in-house constructed program in IDL 6.3.
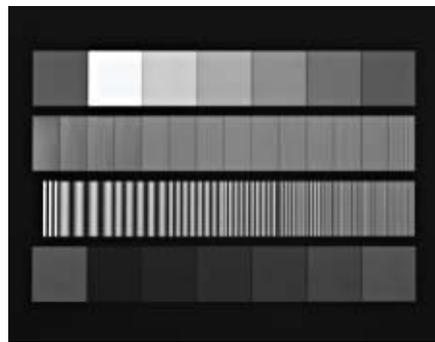
Figure 13: The sinusoidal test target used for distortion correction for the fast laser scanner in the University of Surrey

3.1.5 Octopus IQ

A schematic diagram of the commercial optical CT scanner Octopus IQ is illustrated in figure 14 and the setup is shown in figure 15. Octopus IQ is an evolved version of the original Octopus scanner, which is nearly identical to the first presented optical CT described in section 2.1.1. The Octopus IQ scanner used in the experiments presented in this thesis was located at Aarhus University, Denmark.
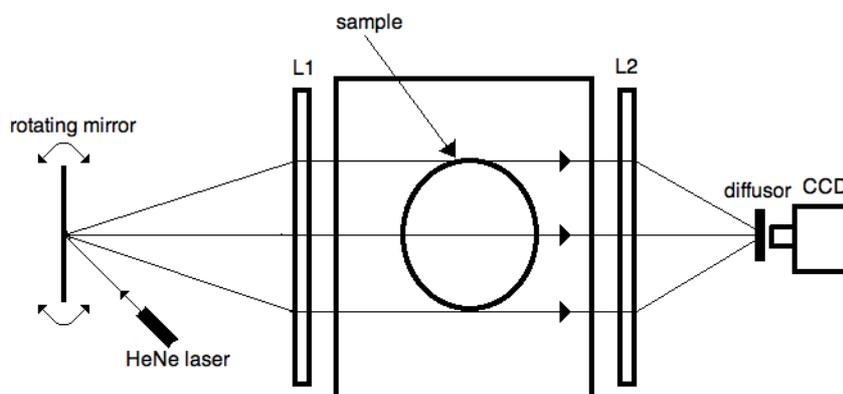
Figure 14: Schematic top view of the Octopus IQ scanner located in Aarhus University, Denmark
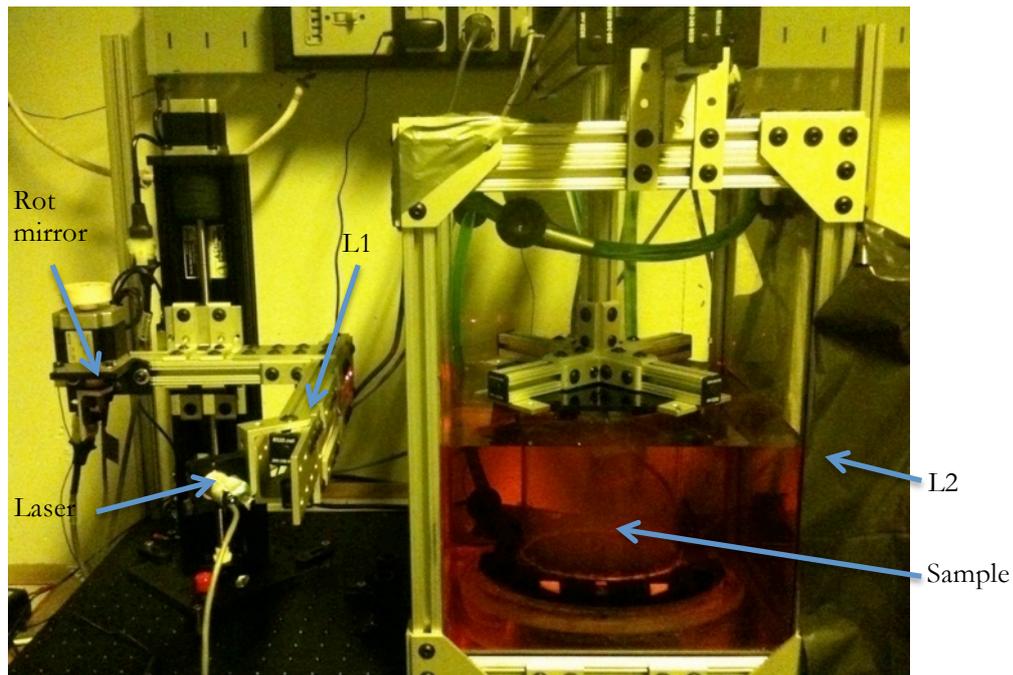
Figure 15: The Octopus IQ scanner. The CCD detector is located outside the photo to the right

The Octopus IQ is a fast laser scanner. A He-Ne laser (633 nm) shines on a fast rotating mirror, which gives rise to a beam that is rapidly moved across the first Fresnel lens, L1. Since the mirror is located in the focal point of a the lens, the beam leaving the lens is parallel to the optical axis. The beam is then transmitted through the glass aquatic tank consisting of the refracting index liquid and the specimen attached on the rotation stage. When the beam exits the tank and reaches the second Fresnel lens, L2, it is focused on a CCD detector behind a diffusor.

Unlike the fast laser scanner earlier described in section 3.1.4, which performs the scanning using the sweeping laser in a rectangular raster approach, the Octopus IQ only scan one slice at a time. Thus, the scanning does not give initial projection images for each angle scanned. Instead, after each completed slice scan, a motor is moving the lenses, laser, rotating mirror and detector vertically to continue next slice scan.

The scanner is driven by software from MGS Research, Inc. called Octopus IQ OCT driver and postprocessing and reconstruction of the projection data is done using modified software provided by MGS Research, Inc. in MATLAB (MathWorks, Natick, MA, U.S.A). The default reconstruction method in the program is filtered back projection using the iradon function with a Shepp-Logan filter.

3.1.6 MRI

The traditional readout method for polymer gel dosimeters is by a T2 weighted MRI sequence (Baldock *et al.*, 2010). Since the R_2 values in the gel are sensitive to temperature gradients, it is favorable to store the gel in the MRI scanner room for some hours before imaging. The MRI

machine used in this thesis was a conventional 1.5 T unit (Symphony, Siemens, Germany) located in Skåne University hospital in Malmö. It is seen in a readout setup of a 3D dosimeter in figure 16. More information about MRI, how it works and the readout of polymer gels can be found elsewhere (McRobbie, 2007; De Deene, 2010).

Figure 16: Siemens Symphony MRI unit in a readout setup with a polymer gel dosimeter

3.2 Dosimeters

3.2.1 Radiochromic film

One way to measure two-dimensional dose distributions in radiotherapy is to use film dosimetry. RCFs is one of the most popular types of films today and are becoming increasingly popular as more complex treatment methods are introduced (Ferreira *et al.*, 2009). This is because of the excellent spatial resolution that comes with the use of a continuous medium, combined with the low energy dependence and good tissue equivalence of the contemporary self-developing RCFs (Kairn *et al.*, 2010).

The type of RCF that has become the standard in radiotherapy QA measurements today is called Gafchromic EBT2 (Jordan, 2010). This film, manufactured by ISP (International Specialty Products Corp., Wayne, NJ, USA), is specifically developed for radiotherapy measurements. It consists of a 30 µm active layer with a radiation-sensitive component between layers of protective polyester over-laminate (International Speciality Products, 2009). When the active components in the film is exposed to radiation, it reacts and forms a blue colored polymer with absorption peaks at 636 nm and 585 nm, thus ensuring a color change of the film relative to the amount of the received radiation. EBT2 film has an effective atomic number of 6.84 (Hartmann et al., 2010) and small energy dependence (1σ=4.5% for 75 kVp-18 MeV photons (Arjomandy et al., 2010)). The film used in this thesis, lot# F12170901A, is presented in figure 17. A sheet can easily be cut to required shape and size (International Speciality Products, 2009).

Figure 17: A sheet and the package of the EBT2 film used in this study

3.2.2 Polymer gel

The selling point of polymer gel dosimetry is the capacity to distinctively record the absorbed dose distribution in a three-dimension volume (Baldock *et al.*, 2010). Because of that, gel dosimetry is particularly advantageous to one and two-dimension dosimeters when to verify dose distributions with steep dose gradients (Baldock *et al.*, 2010). Generally a polymer gel dosimeter contains water, radiation sensitive chemicals (monomers) and a gel matrix substance (Ceberg, 2010) and when it is irradiated, the monomers are polymerized as a function of the absorbed dose. The gel matrix preserves the spatial information by holding the polymers in place.

The dose response for polymer gel dosimeters is due to the formation of the polymer particles that is suspended in the gel after it is irradiated (Baldock *et al.*, 2010). Before irradiation the mobility of the surrounding water molecules bound to the monomers are relatively high, but upon irradiation the molecular mobility is significantly reduced due to the polymerization. This reduction gives rise to a more effective NMR spin-spin relaxation, which is seen as an increase of the R_2 value as a function of the absorbed dose (Baldock *et al.*, 2010). The gel becomes more opaque with irradiation and this partial transparency of the gel lends itself to scanning by optical CT. But since optical imaging of polymer gel dosimeters are characterized by high amount of scattering light, which may deteriorate the measurements, some optical CT scanners might not be suitable for the readout of polymer gel dosimeters.

Numerous articles regarding the use of polymer gel as a verification method in radiotherapy have been published (Vergote *et al.*, 2004; Wuu *et al.*, 2006; Lopatiuk-Tirpak *et al.*, 2008; Ceberg *et al.*, 2010)). A topical review regarding polymer gel dosimetry and various readout systems was recently published (Baldock *et al.*, 2010).

nPAG composition and manufacturing

One of the most thoroughly tested gels and the one used in this thesis is nPAG (De Deene *et al.*, 2006). The gels were mixed in a fume cupboard under normal level of oxygen in a dark environment. The ingredients were pure ionized water (resistivity > 18.2 MΩcm), the matrix substance gelatin (porcine skin, approx. 300 bloom, Sigma Aldrich, St Louis, MI, USA), the two monomers acrylamide (AAm) (electrophoresis grade, ≥99% powder, Sigma Aldrich) and N,N'-methylene-bis-acrylamide (Bis) (electrophoresis grade, ≥98% powder, Sigma Aldrich) and the antioxidant Tetrakis(hydroxmethyl)phosphonium (THP) (techn. ~80% in water, Sigma Aldrich). The quantity of the ingredients in the nPAG gels were 89% w/w water, 5% w/w gelatin, 3% AAm, 3% Bis and 10 mM THP.

The water and gelatin were mixed. To dissolve the gelatin, the mixture was heated up to 45° C. The monomer AAm was added and after 30 minutes, Bis was poured into the mixture. The solution was then left to cool down to about 37° C before THP was added and left to intermix with the compound for about 10 minutes before the gel was poured into the designated containers. The set-up in the fume cupboard is shown in figure 18.

Figure 18: The round-bottomed flask with the gel mixture, the radiator and the thermometer

3.2.3 Radiochromic plastics

A plastic radiochromic material to be used in radiotherapy dosimetry was presented in 2003 (Adamovics, 2003). The dosimeter, called Presage, is commercially available through Heuris Pharma LLC and consists of a solid polyurethane-based material incorporating a radiosensitive leucomalachite green dye (Adamovics *et al.*, 2006). When exposed to ionizing radiation, the dye oxidizes and exhibits a radiochromic response linear to the absorbed dose. This makes the dosimeter darker with an absorption maximum at about 633 nm (Baldock *et al.*, 2010). Unlike polymer gels, Presage is rigid and requires no separable container, which is an attractive feature in

optical imaging since the light then has to pass two fewer interfaces than for polymer gels (Doran, 2009a). Moreover, Presage is insensitive to oxygen and is reasonably tissue equivalent (Z_{eff} = 6.6 compared to adipose tissue at 6.56) (Adamovics *et al.*, 2006). Thus, Presage is considered a very promising material for future verification of radiotherapy treatments (Doran, 2009b). The Presage sample that was used in this thesis is presented in figure 19.

Figure 19: The Presage sample used in this thesis

3.3 Radiochromic film readout

3.3.1 Preparation and irradiation

The EBT2 films, originally 20,3 x 25,4 cm, were cut into pieces of 9,0x9,4 cm and irradiated using 6MV photon beams using a Clinac iX linear accelerator (Varian Medical Systems Palo Alto, CA, USA). The films were placed at a depth of 10 cm (SSD 90 cm) and solid water (RW3, PTW, Freiburg, Germany) was used as build-up material. The treatment planning was carried out using Eclipse 10.0 with AAA. The films were irradiated with various fluence-modulated fields as well as conventional fields with a maximum size of 8x8 cm. Calibration films were irradiated with a 15 x 15 cm field for doses between 0.2 and 2.5 Gy. The maximum calibration dose were about 25% higher than the maximum dose used. Two films were kept unirradiated and these are called background films from now on.

3.3.2 Readout – flatbed

After about 24 hours post irradiation, the films were scanned using the Epson 4990 Photo flatbed scanner using a recommended scanning procedure (van Battum *et al.*, 2008). The films were placed with the short side of the original film sheet parallel to the short side of the scanner (i.e. in portrait mode). It has been showed that the scanner response is most uniform in the center (van Battum *et al.*, 2008), thus a cardboard frame was used to place the films at the same location in the middle of the scanner. The scanning was carried out using the Epson Scan software in professional mode with all filters and image enhancements turned off. The films were scanned in transparent mode, as "positive" with a scan resolution of 72 dots per inch (0.35 mm/px) and a color depth of 48-bit RBG with 16 bits per channel. These settings acquire images using three channels, each containing the signal from wavelengths 400-500 ("blue" channel), 500-

600 ("green") and 600-700 nm ("red"). Three scans were carried out for each film and three light field images, i.e. scans without any film, were acquired prior to and after the film scanning. These images were subsequently averaged. To take into account potential warming up effect that occurs after the scanner is turned on, the scanning of the films started after ten successive scans without any films in place.

All the scanned film images (tiff format) were imported into MATLAB for processing purposes. The red channel pixel value were extracted from each image and converted to absorbance values by taking the logarithm of the pixel-by-pixel division between the light field and the film, as described by formula (1). Then the net absorbance was yielded by subtracting the absorbance for a film with the mean value of the absorbance from a region in the center of a background film. A fourth degree polynomial was applied to the net absorbance values and the corresponding prescribed dose from the TPS for a mean value in a central ROI in each of the calibration films. The calibration curve was then used to calibrate all films from net absorbance to absorbed dose. Eventually the images were resized to a resolution of 1x1 mm² with a 3x3 box-shaped kernel using the "imresize" MATLAB function. The dose images from the TPS were linearly interpolated from 2.5x2.5 mm² to the same resolution.

3.3.3 Readout – CCD scanner and flat panel approach

Even though the Surrey CCD scanner and the flat panel approach have different setups, the imaging was carried out in the same way. Each film was positioned in an in-house built frame made of black painted Lucite (figure 20). The frame was screwed to a lab jack and positioned at the place of the refractive index container. All imaging were acquired in a dark room to dispose of potential stray light. The CCD chip was cooled down to -55° C before the start of the image acquisition to minimize the thermal noise.

Figure 20: The frame used for the EBT2 films in optical CT scanners

For both the original parallel beam CCD scanner and the flat panel approach, projections with 512x512 pixels were acquired. Since the rotation stage was removed from the original 3D readout setup, one projection was equivalent to one film readout. All the films were read out three times each and subsequently averaged. Light field images were taken on the frame without any film in

place prior to and after the film imaging and dark field images were acquired with the lens cover preventing any light from entering the CCD chip.

All the images were imported to MATLAB and processed. Equation (3) was used to get absorbance images of all the films and the net absorbance images were obtained by subtracting the absorbance image of an unirradiated film from the absorbance images of the irradiated ones. Net absorbance was converted to absorbed dose by using a calibration curve, following the same approach as described earlier in section 3.3.2. As the films were to be compared to the films read out using the flatbed scanner and the TPS data, the images were all resized to 1x1 mm² resolution with a 3x3 box-shaped kernel using the "imresize" MATLAB function.

3.3.4 Readout – Octopus IQ

The frame with the film was put into the Octopus IQ in the container showed in figure 15. The image acquisition software from MGS research was un-rewriteable and scanned by default one horizontal slice in a 3D volume at a time. That meant that a row of the film had to be scanned 300 times before going on to the next (a full slice consisted of 300 projections). That led to a total scan time of about 25 minutes for 7 cm film (70 slices).

Two scans were performed, one of a film and one light field scan. The scans were carried out in the dark using default settings and identical parameters were used for both scans. The raw data were imported to MATLAB for further processing. Equation (1) was used to convert the raw data to absorbance images. The scans were only evaluated using absorbance measurements since the access to the scanner was limited.

3.4 Polymer gel readout

3.4.1 Preparation and irradiation

An amount of 2.7 liters of nPAG gel was manufactured as described in section 3.2.2, and poured into an acrylic cylindrical container (Ø 15 cm, length 17 cm). A lid shut the container and it was then left to set. Five small acrylic glass vials (Ø 2.7 cm, length 1.8 cm) were also filled with gel from the same batch. The vials were irradiated with 0, 1, 2, 3 and 4 Gy respectively, to ensure the linearity of the gel batch.

Approximately 24 hours after the gel was manufactured, it was CT scanned (Mx8000 IDT 16, Philips Medical Systems, Eindhoven, the Netherlands) with the cylindrical axis perpendicular to the couch and the data were imported into Eclipse TPS. The additional dose from the CT scan was considered negligible (~10 mGy) in relation to the absorbed dose given when irradiated on the linear accelerator. The gel was labeled with two markers on the bottom to ensure that the forthcoming slice-by-slice reference subtraction for the optical CT was done within a degree of

rotation of a reference position. A four-field box with 3x3 cm 6 MV photon beams (0°, 90°, 180° and 270°) was planned on the CT data. The prescribed dose to the four-field box was 3 Gy, delivered with a dose rate of 600 MU min^{-1} using 95-97 MU per beam. Irradiation was carried out using a Varian Trilogy Tx linear accelerator. The irradiated gel is seen in figure 21 with arrows illustrating the beams' trajectories.

Figure 21: The gel irradiated with a four-field box. The arrows illustrates the directions of the beams

3.4.2 Readout – Octopus IQ

Identical scans were performed pre- and post-irradiation with the gel placed upright on exactly the same position, using default Octopus IQ OCT driver settings to control the motors and detector. After irradiation, the gel was left to polymerize for 16 hours before the optical CT scan was initialized. A number of 300 projections with 145 slices, each divided on 180°, were acquired with a total scan time of approximately 48 minutes. The pre-irradiated gel scan was used as a reference set and divided by the second scan in a post-processing step to cancel potential defects in the gel itself. Throughout the scanning process, a dark environment was maintained to minimize the effects of stray light that possibly could contribute to the signal in the detector. The refractive index liquid used was optimized for polymer gel dosimeters and based on a mix of glycerol, water, sugar and a dye.

Reconstruction gave slices with 1x1x1 mm³ resolution and units of OD, which was converted to relative absorbed dose by normalization to a region in the center of the four-field box using MATLAB. A 3x3x3 box-filter was applied to smooth the raw data.

3.4.3 Readout – MRI

Approximately 24 hours after irradiation, the gel was scanned lying down using MRI. The image acquisition was carried out using a 32-echo multi-spin echo sequence with 25 ms echo time and 9780 ms repetition time. The voxel size was 1x1x3 mm³ with two averages and four concatenations. The imaging time was 5,5 hours.

In-house developed software was used to create R_2 maps from the MRI data and the additional image processing was done using MATLAB. The R_2 maps were converted to relative absorbed dose by background subtraction and normalization to a central volume in the four-field box. The dose distribution was linearly interpolated to 1x1x1 mm³ (as was the dose images from the TPS with an original resolution of 2x2x2 mm³). The raw data was then smoothed with a 3x3x3 box-filter.

3.5 Radiochromic plastics/polymer gel readout

3.5.1 Preparation and irradiation

An nPAG gel was manufactured and poured into two identical 0.5 l cylindrical glass containers (Ø 8 cm, length 12 cm) and five 15 ml glass vials. One of the two large containers was left unirradiated and later used to obtain a background R_2 value for the irradiated gel. The small vials were irradiated with 0, 1, 2, 3 and 4 Gy. Immediately after manufacturing, the gels were left to set in the dark for about 24 hours in room temperature. A Presage sample (Ø 6 cm, length 6 cm) was procured and wrapped in two layers of 0.5 cm thick SuperFlab bolus material to achieve the same thickness as the gel container. Both the gel and Presage sample were CT scanned (LightSpeed RT, GE Healthcare, Milwaukee, WI, USA) and the CT images were imported to the TPS where the same VMAT (RapidArc) prostate plan was planned on the two dosimeters. The additional dose from the CT scan was considered negligible (~10 mGy) in relation to the absorbed dose given when irradiated on the linear accelerator. A clinical RapidArc plan was used to receive clinically relevant dose modulation, however, the prostate target was reduced in size to fit into the small Presage sample by some margin. The target dose was prescribed to 3 Gy, given with one full clockwise arc rotation and a collimator rotation of 30° using 450 MU and a varying dose rate between 200 and 600 MU/min.

Figure 22: The Styrofoam support supporting the Presage sample covered by two layers of SuperFlab

A Clinac iX linear accelerator (Varian Medical Systems) was used to deliver the RapidArc plans. The dosimeters were placed in the same position as in the CT scans, using a Styrofoam support (figure 22). Due to insensitive response to absorbed dose in the Presage sample, three identical

dose deliveries were carried out consecutively. A photo of the irradiated gel is shown in figure 23.

Figure 23: The gel irradiated with a small RapidArc field

3.5.2 Readout – CCD scanner

The Presage sample was placed on the rotation stage and lowered into the container with the refractive index liquid (2-Ethylhexylsalicylat and a few drops of green dye). A number of 400 projections were acquired with a resolution of 256x256 pixels divided on 180° for a total scan time of about 25 minutes. To get light field images, the sample was raised from the container and 50 projections were acquired. Finally, ten dark field projections were taken with the lens cap on the camera.

Equation (3) was used to create absorbance maps of the projections. The light field image was acquired by averaging 50 light field projections and the dark image was acquired by averaging 10 dark field projections. The absorbance data was reconstructed using filtered back projection with a Ram-Lak filter. To reduce the optical and reconstruction artifacts, a 5x5x11 box-filter was applied. In MATLAB, linear interpolation to increase the pixel side from 0.3 mm to 1 mm was carried out and the resulted matrix were smoothed with a 3x3x3 box-filter. To be able to compare the data to the TPS, the latter was linearly interpolated from 2.5x2.5x2 mm^3 to 1x1x1 mm^3.

3.5.3 Readout – Fast laser scanner

The same container and rotation stage as described in section 3.5.2 was used when carried out scanning with the fast laser scanner. The sample was immersed in the same way as well. The scanning was performed with 400 projections over a rotation of 180° for 256x256 projections in

about 25 minutes. After the projection acquisition, the sinusoidal test target (figure 13) was imaged using identical parameters.

The projections were converted to absorbance maps and distortion corrected using the methodology described in section 3.1.4. Due to the small size of the test target, only approximately half the sample could be corrected for distortion. Reconstruction, filtering and interpolation was done in the same way as described in section 3.5.2, but with a 5x5x9 box-filter instead of 5x5x11.

3.5.4 Readout – MRI

Scanning of the gel with MRI was carried out 24 hours post irradiation. A 32-echo multi-spin echo sequence was used with the following parameters: echo time 25 ms, repetition time 6000 ms, voxel size 1x1x3 mm^3, two averages and four concatenations. The scan time was 1 hour and 43 minutes. A smaller part of the unirradiated gel was scanned with the same parameters to obtain a background R_2 value.

R_2 maps were acquired using in-house software and these maps were subsequently post-processed using MATLAB. The conversion from the R_2 map into relative absorbed dose, as well as normalization and interpolation was carried out as earlier described in section 3.4.3.

4. Results and discussion

The results from the measurements are presented below. Section 4.1 addresses the readout of the Gafchromic EBT2 films using a standard flatbed scanner and different optical CT's. In section 4.2, comparisons between MRI readouts and Octopus IQ readouts of a polymer gel dosimeter are made. In section 4.3, the combination polymer gel dosimeter and MRI are compared to an identically irradiated Presage and optical CT combination. For all the measurements, the TPS-calculated dose distributions are used as reference.

4.1 Radiochromic film readout

Since the manufacturer recommends using a flatbed scanner to digitize EBT2 films, it is used as reference modality in these measurements. A flatbed scanner dose image and a parallel beam scanner dose image acquired from a conventional 3x3 cm beam irradiated on an EBT2 film are presented (figure 24 a) and b)). The absorbed dose profiles extracted along the dotted lines in an overlay of the two dose images showed poor agreement with a mean value about 8% smaller for the optical CT dose image (figure 24 c) and d)). Images of films acquired using intensity-modulated irradiation were investigated in the same way, together with corresponding dose profiles from the TPS (figure 25 a-d)). The agreement was unsatisfied for the parallel beam

scanner with a mean deviation from the TPS data larger than 6%, while the flatbed scanner image profiles coincided well with the TPS (less than 2% mean deviation from the TPS data). However a similar dose intensity pattern was seen for all scanners and the TPS.

The films read out using the parallel beam scanner exhibited more noise in the dose images than the films read out using the flatbed scanner. Furthermore, the dose sensitivity was generally lower using the parallel beam scanner readout method. These results indicate that the parallel beam scanner needs major development if it should be used for film dosimetry.
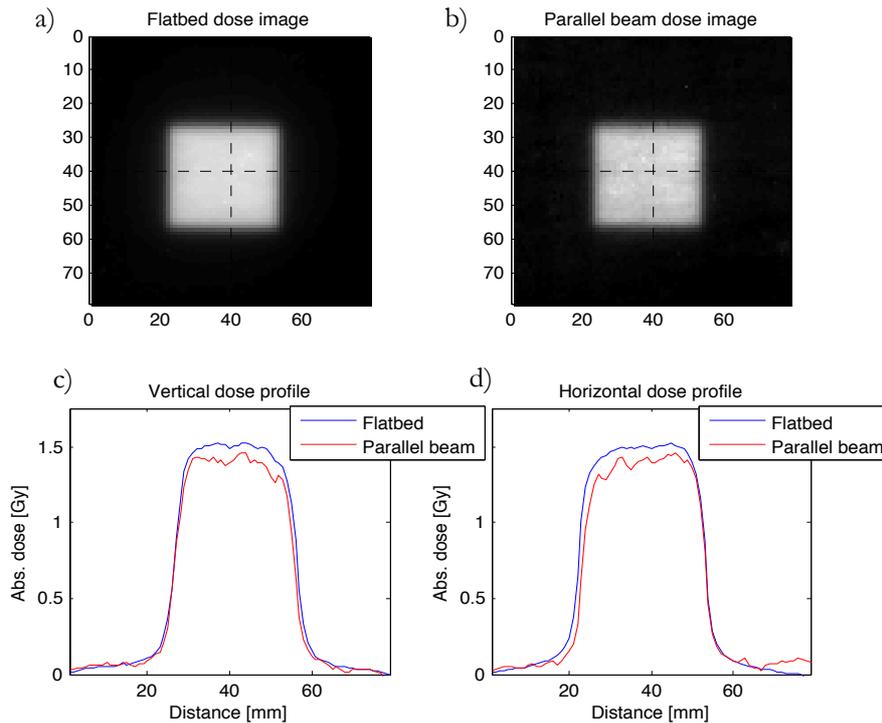
Figure 24: Dose images from a 3x3 cm field irradiated on an EBT2 film and read out using a) flatbed scanner and b) the parallel beam CCD scanner. c) vertical and d) horizontal line profiles from the dotted lines in the dose images

Corresponding evaluation of the films presented in figure 24 and 25 was carried out using the flat panel approach instead of the parallel beam scanner. The dose image and absorbed dose profiles of the film irradiated with a conventional 3x3 cm beam showed excellent agreement between the flatbed scanner and the flat panel approach and the dose deviation was within 1% (figure 26). As for the film irradiated with an IMRT field, both an overlay of the 1 Gy isodose lines (figure 27) and absorbed dose profiles (figure 28) agreed well between the two modalities and the TPS and showed a mean dose deviation of less than 2%.
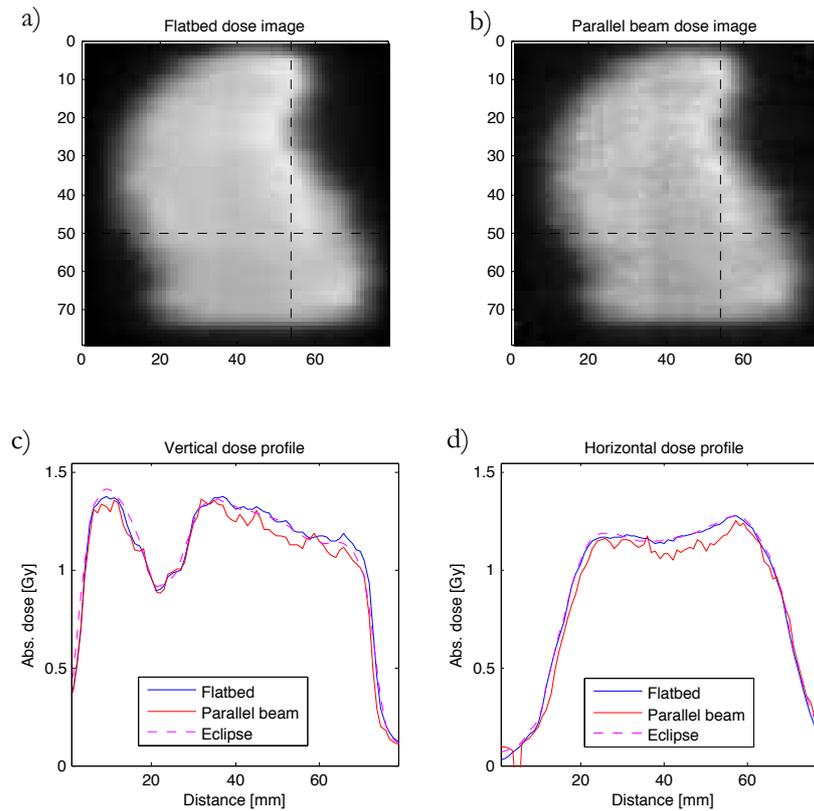
Figure 25: Dose images from a small IMRT field irradiated on an EBT2 film and read out using a) flatbed scanner and b) the parallel beam CCD scanner. c) vertical and d) horizontal line profiles from the dotted lines in the dose images together with the corresponding line profile from the TPS

The setup for the flat panel approach (figure 9) is very provisional as of this writing, which means that further development is needed to enable frequent use for film dosimetry. Development needed includes a stable arrangement, a larger LED screen and perhaps scatter correction. Although no scatter measurements were conducted, it is likely that the setup of the flat panel approach suffer more from scattering light than the flatbed scanner because the light has to travel a longer distance. A similar method using an optical CT for film scanning has been carried out with the cone-beam Vista scanner (section 2.1.2) (Babic *et al.*, 2010). To take into account the film scattering, it is suggested that a complex multiple grid approach will be needed in order to achieve quantitative densitometry.
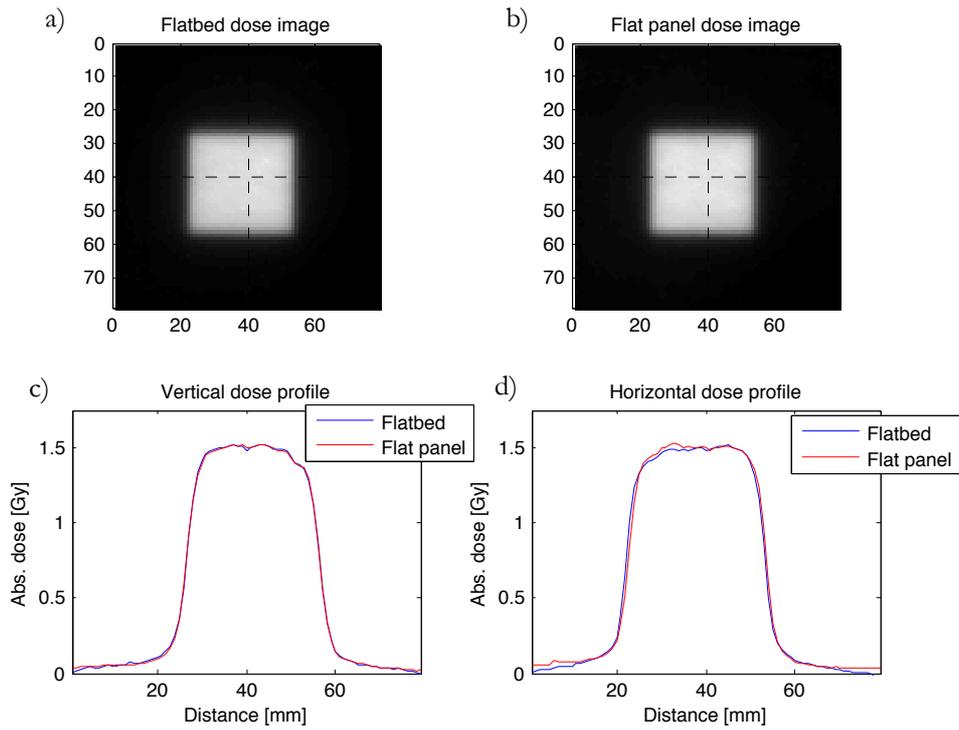
Figure 26: Dose images from a 3x3 cm field irradiated on an EBT2 film and read out using a) flatbed scanner and b) the flat panel approach with the parallel beam CCD scanner. c) vertical and d) horizontal line profiles from the dotted lines in the dose images
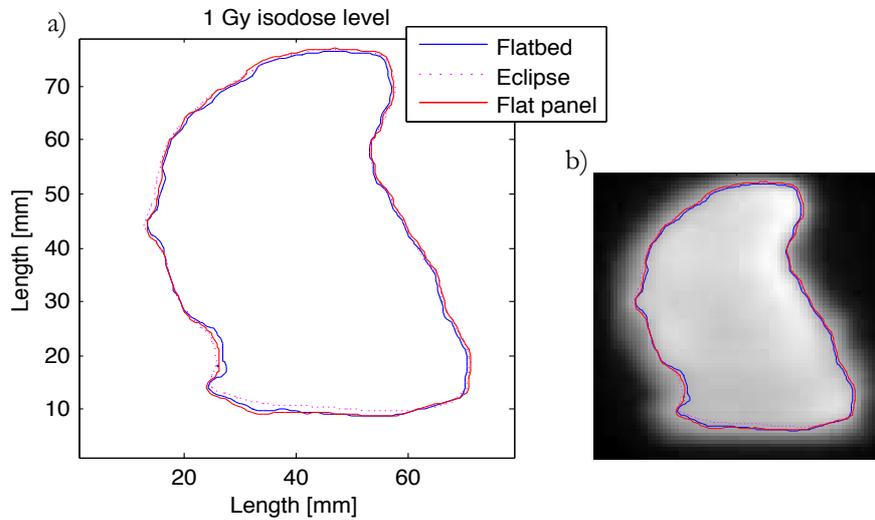

Figure 27: a) 1 Gy isodose level for the dose images in figure 27. The dotted line is the corresponding isodose level from the TPS. b) The same isodose level presented together with the dose image from the TPS
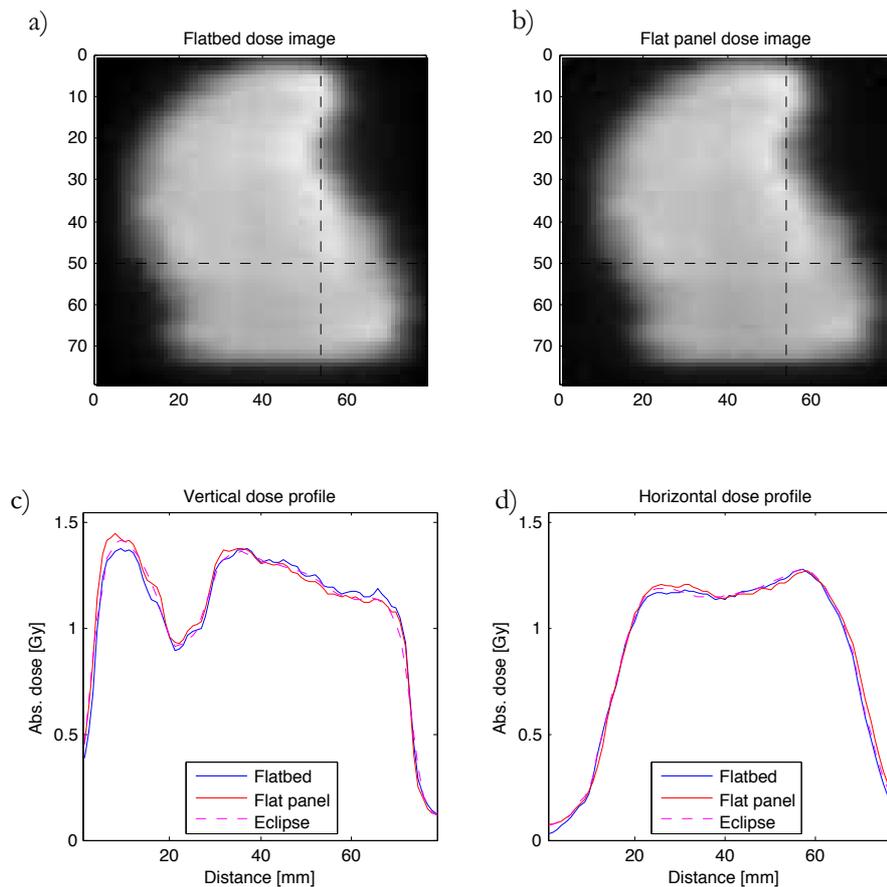
27

Figure 28: Dose images from a small IMRT field irradiated on an EBT2 film and read out using a) flatbed scanner and b) the flat panel approach with the parallel beam CCD scanner. c) vertical and d) horizontal line profiles from the dotted lines in the dose images together with the corresponding line profile from the TPS

Film scanning using laser scanners was not tested as thoroughly as the parallel beam scanner due to lack of calibration film scans, but absorbance images were acquired from both the Octopus and flatbed scanner. The normalized absorbance line profiles showed mean discrepancies of about 0.05 normalized absorbance units (figure 29). Much more measurements are needed to say whether film dosimetry using the Octopus scanner is feasible or not. However, the absorbance image from Octopus presented with an overlay of the 70% level of the maximum absorbance for both modalities showed excellent agreement with a deviation within sub-millimeters (figure 30). No films readout using the fast laser scanner is presented, but since it share many of its properties with the Octopus scanner, it is likely that they would have the same potential difficulties.

a) OCTOPUS absorbance image   b) Flatbed absorbance image

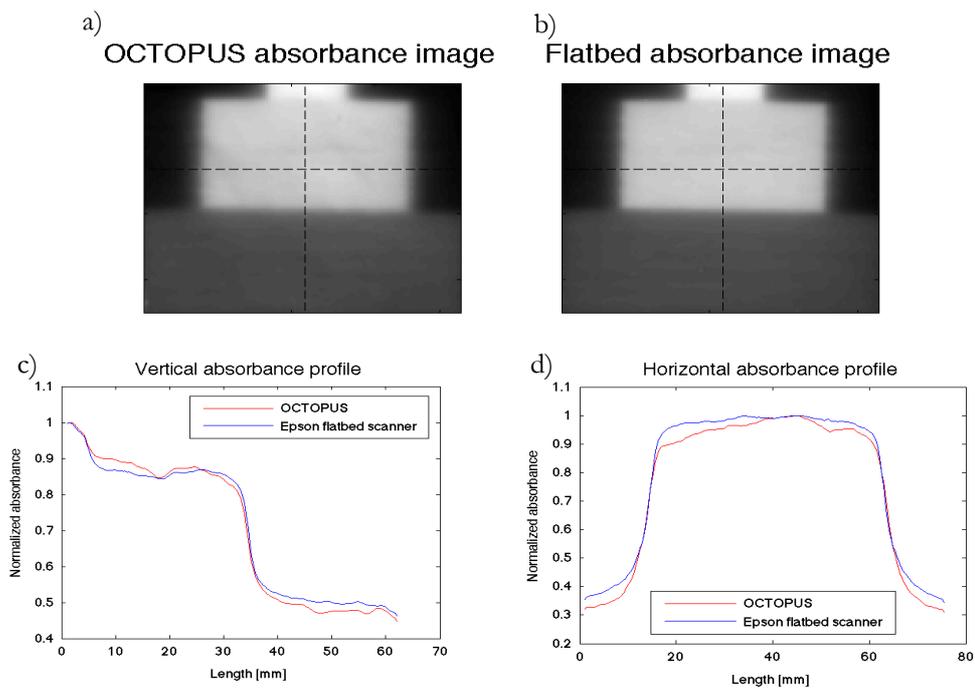c) Vertical absorbance profile   d) Horizontal absorbance profile

Figure 29: Absorbance images from a fluence modulated pyramidal field irradiated on an EBT2 film and read out using a) the Octopus IQ scanner and b) a flatbed scanner. c) vertical and d) horizontal line profiles from the dotted lines in a) and b)

OCTOPUS absorbance image
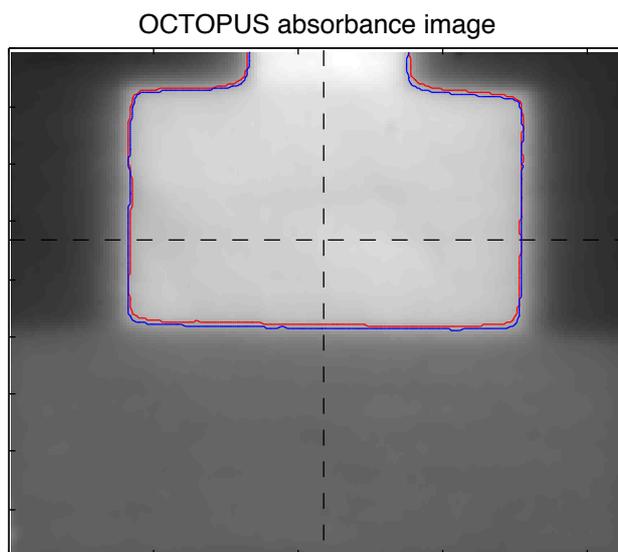
Figure 30: The absorbance image from figure 29 a) and overlay of the 70% isodose level from readouts with Octopus IQ (red) and the flatbed scanner (blue)

Laser scanners can provide the highest response with the EBT2 film because of the wavelength of the laser at 633 nm, which is close to the peak absorbance of the film (International Speciality Products, 2009). However, laser scanners can produce artifacts due to the in ... al Speciality Products, 2009). Thus, one has ... dosimetry.

Gafchromic EBT2 replaced EBT in 2009 and while the original version was considered a reliable instrument in film dosimetry (van Battum *et al.*, 2008; Hartmann *et al.*, 2010), various publications have addressed problems with its successor (Hartmann *et al.*, 2010; Kairn *et al.*, 2010). These mention intrinsic film heterogeneities as the main source of error. To get rid of these issues, it is suggested that the way of handling the readout of EBT2 is to scan the film both prior to and after the irradiation (Kairn *et al.*, 2010). Unfortunately, it was not possible to follow this recommended methodology in this study, but since this experiment is a pure comparison between readout modalities it should not matter as long as the course of action is the same for all scanners. Another aspect that should be mentioned is the fact that the scanner signal from the flatbed scanner is a function of the lateral position (van Battum *et al.*, 2008). This is mainly a problem when scanning larger films, so for the small pieces used in this study no lateral effects could be perceived.

4.2 Polymer gel readout

The MRI readout method is time consuming, which is one of the reasons why the use of the optical scanners is increasing. However, the polymer gel/MRI is an available true 3D dosimetry system and is thus working as the reference for the optical scanner readouts." Overall, good agreement was found between the readouts of the polymer gel, irradiated with a simple 3x3 cm four-field box, carried out with MRI and the Octopus scanner, respectively (figure 31). The 85% isodose surfaces obtained from the two readout modalities were compared by extracting a slice from an overlay of the two investigated volumes together with a slice from an overlay of the volume calculated by the TPS (figure 31 c)). It is seen that the MRI readout was more consistent to the TPS data.

To investigate the dose difference between the three different data set of the four-field box, the volumes were positioned in approximately the same position, thus excluding any possible set-up variations. The relative absorbed dose differences were calculated voxel-by-voxel within a volume of interest, i.e. a volume enclosed by the 90% isodose surface. Relative dose difference histograms for Octopus versus TPS, MRI versus TPS and Octopus versus MRI (X versus Y means that Xvoxel(i)-Yvoxel(i) in the VOI90% of Y) are presented (figure 32). The mean deviation for Octopus versus TPS, MRI versus TPS and Octopus versus MRI were (-0.62 ± 3.0)%, (-0.30 ± 2.9)% and (-0.78 ± 2.9)% respectively. Thus, all dose volume comparisons showed good agreement with a mean value within 1% and a standard deviation of about 3%.
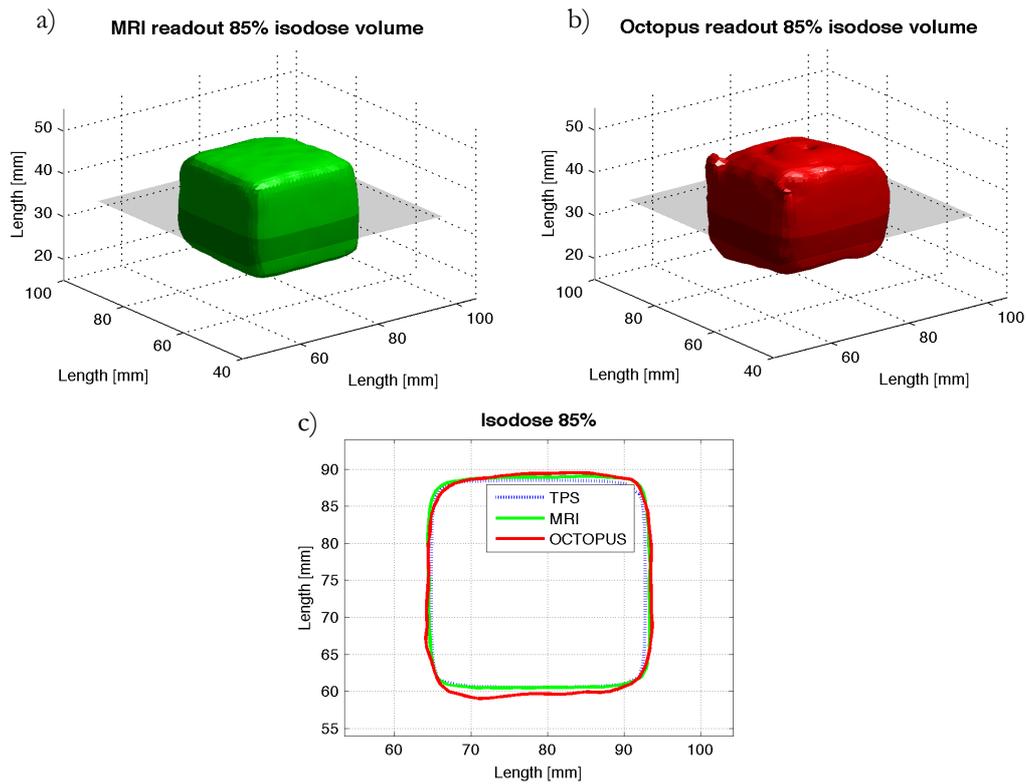
Figure 31: Isodose volumes of the four-field box irradiated on a polymer gel dosimeter from a) MRI and b) Octopus IQ readout. c) Contours of the dark slices in a) and b) and the corresponding slice from the TPS
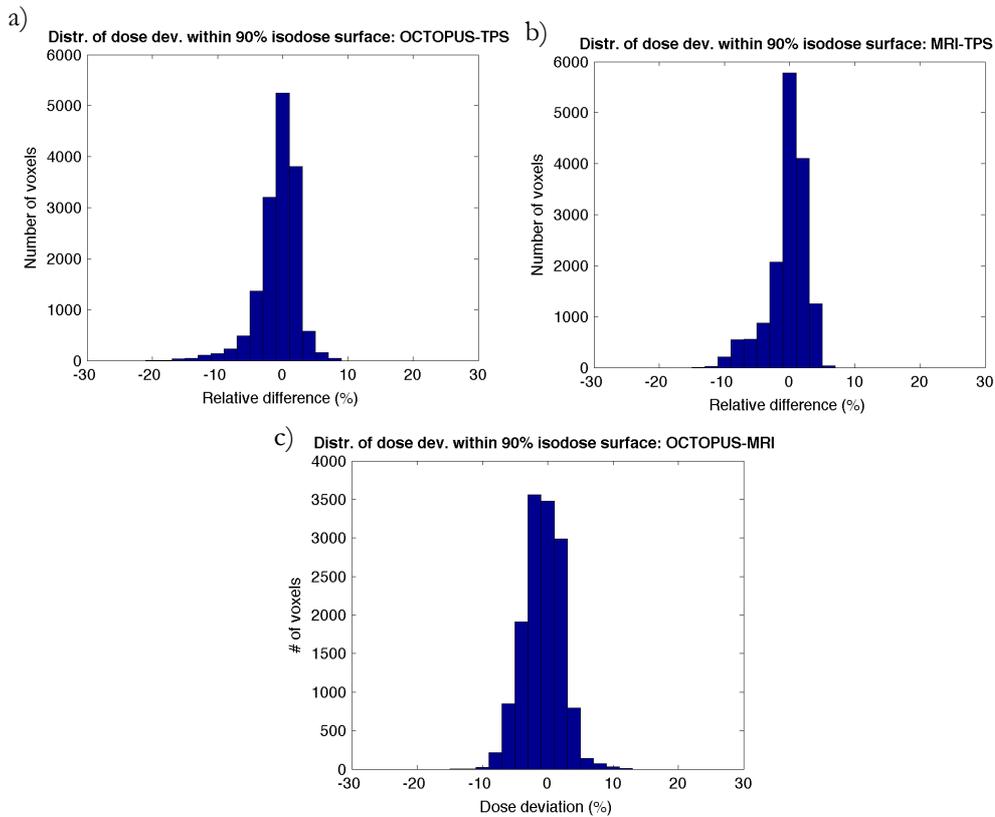
Figure 32: The distribution of voxel-by-voxel dose deviations for the four-field box field in a volume enclosed by the 90% isodose surface. a) Comparison between the Octopus IQ readout and the TPS. b) Comparison between the MRI readout and the TPS. c) Comparison between the Octopus IQ readout and the MRI readout

There are some things that need to be considered before any conclusions can be drawn from this experiment. The gel manufactured for the experiment was poured in a large flask and it is possible this resulted in a weak gel matrix. If that was the case, it is plausible that the very rapid rotation of the sample in Octopus IQ gave rise to artifacts in the data presented in figure 31 and 32. The slanting volume of the Octopus data could also be explained with the fact that the gel was irradiated and MRI scanned with the base of the flask perpendicular to the couch, while the Octopus readout was performed with the flask standing up. Since the gel might have been unfirm, this could have lead to monomers that was irradiated in one position changed place from irradiation to readout.

The background R_2 value was taken from slices in the irradiated gel and not from an unirradiated gel, which is usually done (Ceberg, 2010). Another thing that should be considered with the MRI readout is that a slice thickness of 0.3 cm was used scanning the gel that was irradiated with a 3 x 3 cm beam. This means it could be possible that the slices ended up in an inconvenient way, so that the thickness of the slices blurred the edges and made the high dose volume smaller after interpolation. This could be the reason for the skewed appearance of the distributions in figure 32 b) and c).

The vials irradiated when carrying out polymer gel measurements were not used to calibrate the gel to absorbed dose. Instead they were used to control the linearity between the R_2 value and optical density of the gel and the absorbed dose for each batch of gel. For both batches tested in this study (the gels in 4.2 and 4.3), the dose response was confirmed to be linear in the relevant dose range, which meant that the background subtracted R_2 data and optical density could be directly translated to relative absorbed dose. Using this methodology (suppose linear dose response and subtract the background) leads to a standard uncertainty in absorbed dose of about 3% (Karlsson, 2007).

No gel measurements were done with the scanners from the University of Surrey. The fast laser scanner is in many ways similar to the Octopus scanner, which means that gel readout should be possible. Gel readout using the CCD scanner on the other hand is very difficult (S. Doran, pers. comm.). When irradiated, the gel changes refractive index considerably and that leads to big signal losses in the projections with the CCD scanner.

4.3 Radiochromic plastics/polymer gel readout

The same RapidArc plan was delivered to a polymer gel and a Presage sample. As described earlier in this work, polymer gel dosimeters read out by MRI is a method well known and it could therefore be seen as a reference to the readouts of the Presage sample by the optical CT scanners."

The MRI readout of the gel showed very good agreement to the TPS (figure 33). The 90% isodose volume read out with MRI and calculated by the TPS, respectively, are presented (figure 33 a) and b)), as well as the isodose lines from a slice extracted from an overlay of the two volumes (figure 22 c)). The relative absorbed dose differences between the two volumes calculated voxel-by-voxel within the volume enclosed by the 90% isodose surface, resulted in a mean value much lesser than 1%. More accurately, the mean value and standard deviation were (-0.16 ± 2.2) %. The distribution of the deviations is illustrated in a histogram (figure 33 d)).

The vials irradiated to different doses in connection to the plastic irradiation were used in the same way as described in section 4.2.
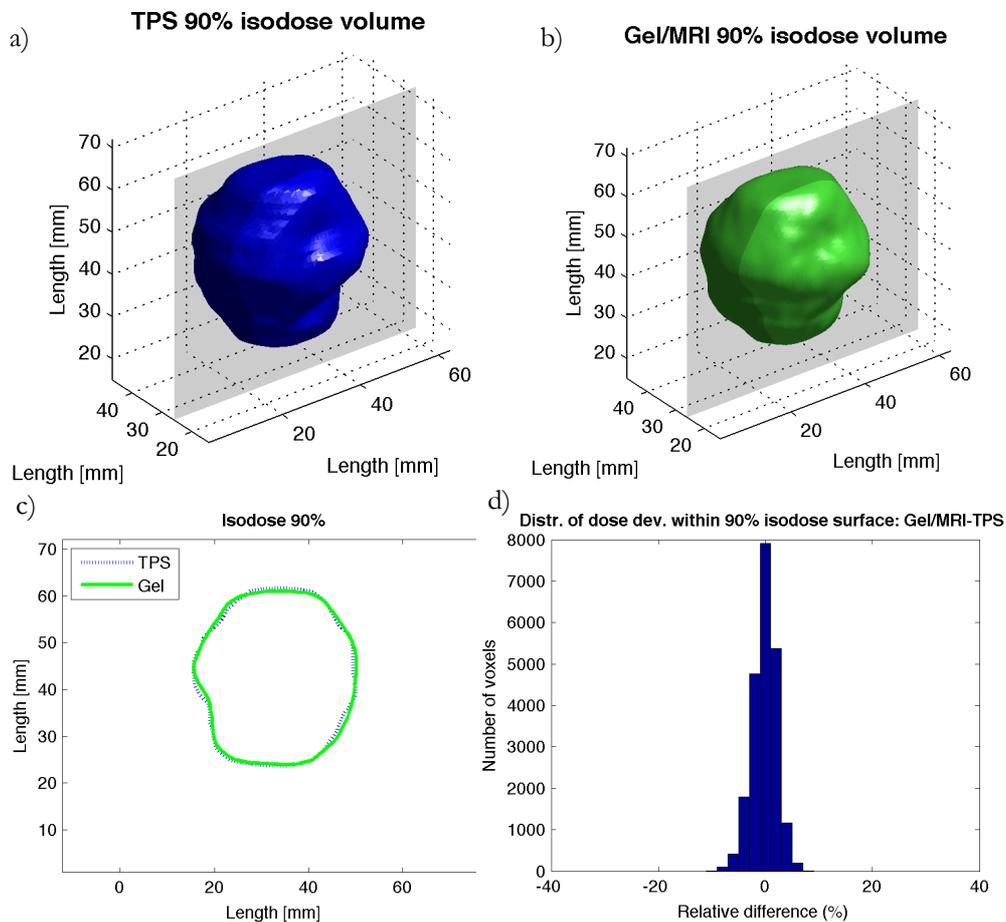
Figure 33: The 90% isodose surface projected into a 3D view for a) the TPS and b) gel read out by MRI. c) Contours of the dark slices in a) and b). d) Distribution of dose deviations inside the 90% isodose volume

The CCD scanner readout of the Presage sample irradiated with the same field as the gel in figure 33 is presented (figure 34). Unfortunately, due to inhomogenous light field that resulted in a signal loss in the absorbance projections, a gap was formed inside the measured volume (figure 34 d)). Projections from an unirradiated sample from the same batch instead of the constant light field (see equation (3)) were also tested without any improvement in the reconstruction. A better

alignment of the scanner, i.e. a more homogenous light field, is needed to make more accurate comparisons between the TPS and the CCD scanner. Nevertheless, when comparing the calculated and the measured isodose surfaces outside the data loss volume, e.g. at a 60% isodose surface, a similarity could be perceptible (figure 34 a) and c) respectively b) and d)). Thus, these first experiments indicate that the CCD scanner has a potential to carry out 3D dosimetry.
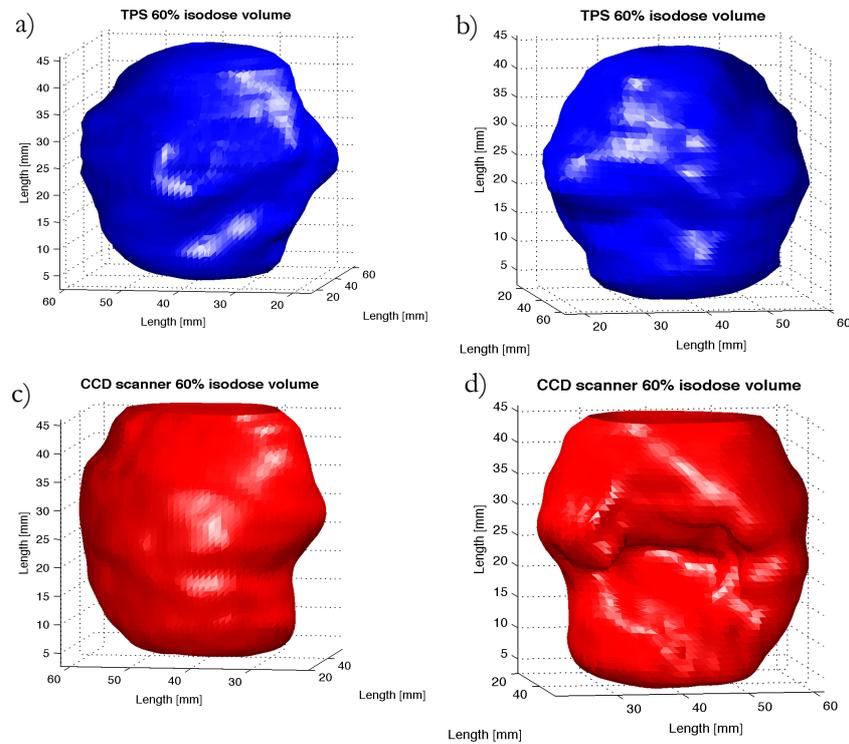

Figure 34: a) and b) The 60% isodose volume in different angles for the TPS. c) and d) The corresponding isodose volumes for a Presage sample read out using the parallel beam CCD scanner from the University of Surrey

A comparison between the Presage sample read out with the fast laser scanner and the corresponding dose volume calculated from the TPS was carried out, but due to limitations in the distortion correction, only approximately half the irradiated volume is presented (figure 35). The two volumes, presented at 80% isodose volume, share the same features (figure 35 a) and b)). However, the 80 % isodose level from a slice extracted from an overlay of the investigated volumes showed that the measured volume was smaller than the one calculated in the TPS (figure 35 c)). The distribution of dose deviations for the fast laser scanner versus the TPS resulted in a mean deviation of (-1.9 ± 10.3) % within the volume enclosed by the 90% isodose surface. The skewed appearance of the distribution suggests that the volume measured was smaller than the one from the TPS as well (figure 35 d)).

The optomechanical complexity of the scanner requires very accurate alignment to work properly and if that was not achieved, it is possible that the beam in some spots missed the detector and

gave lower signal in some positions in the projections. This could be one explanation to the divergence between the investigated volumes. It is also possible that there were some problems with the Presage sample used. It is known that the radiochromic response will fade over time (Adamovics *et al.*, 2006) and since the sample used came from a fairly old batch (approximately two years), an inhomogenous response of the dosimeter cannot be excluded.
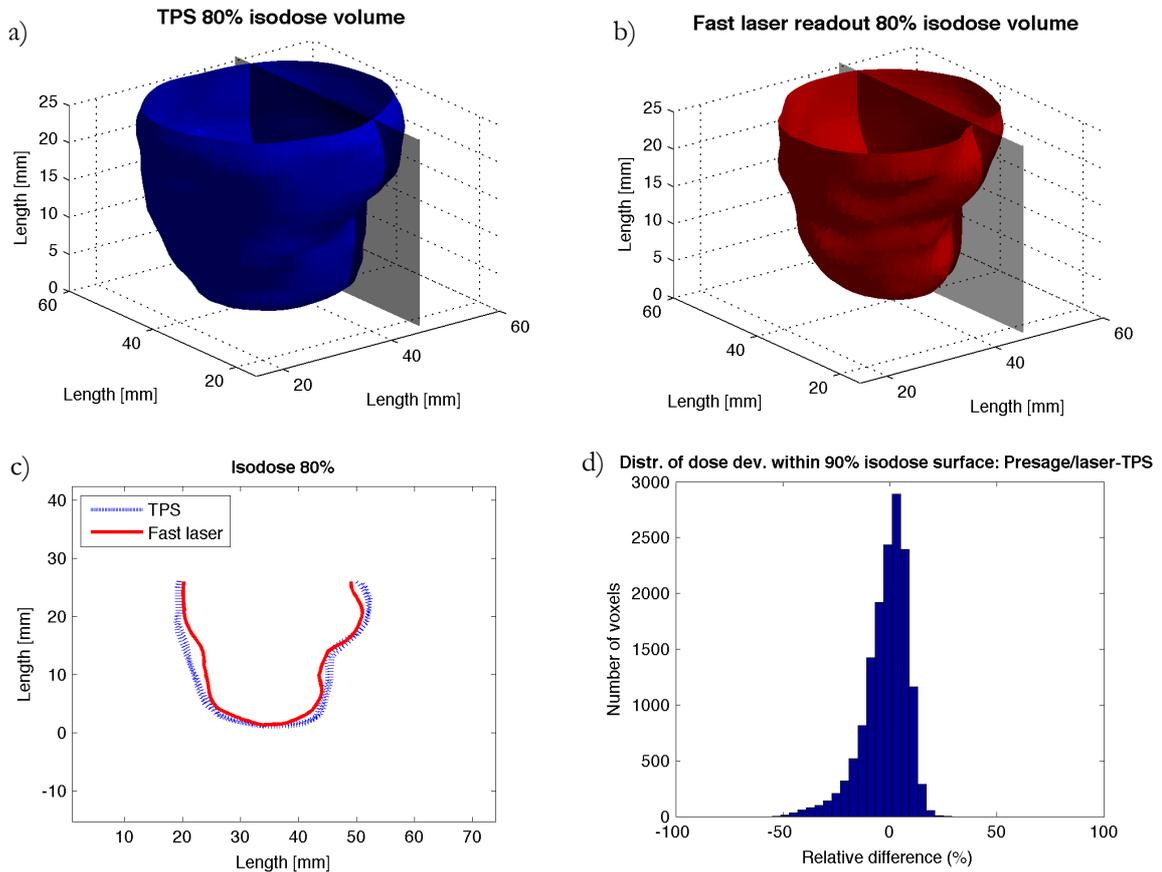
Figure 26: The 80% isodose surface projected into a 3D view for a) the TPS and b) a Presage sample read out by the fast laser scanner from the University of Surrey. c) Contours of the dark slices in a) and b). d) Distribution of dose deviations inside the 90% isodose volume from the TPS

For future experiments, improvement regarding the image acquisition should be made. For instance, the index-matching liquid should be optimized for the specific sample used. If not, dark stripes in the edges of the projections can be visible. This image artifact was present during these experiments, which forced the useful FOV to be decreased. It is recommended to do a scan of the sample both prior to irradiation and afterwards (Doran, 2010). Unfortunately, that was not possible in this study. All reconstructions was done using filtered back projection and that could possibly be improved by reconstructing algebraic (ART) (Doran, 2009b).

5. Conclusions

An evaluation of three different optical CT scanners was conducted. The purpose was to develop and investigate their potential as multi-purpose scanners for both 2D and 3D dosimetry. The detector systems used during the readout evaluation were RCFs (Gafchromic EBT2), polymer gel dosimeters (nPAG) and radiochromic plastics (Presage). The measurements performed in the study were done solely for the purpose of testing the optical CT scanners to see if it could be possible to use any of them as a multi-purpose scanner. Consequently, this was no test of the different dosimeters or delivery techniques themselves.

For the modalities investigated both 2D and 3D detector systems were read out. Some scanners showed potential to read out all used detector systems, some need major development and some did not meet the minimum requirements (table 1). Due to logistic issues, a complete comparison with all of the scanners in all experiments was not achievable within the scope of this study.

Table 1: A summary of the results in this study

Readout modalities					
	Parallel beam CCD	Flatbed	Octopus IQ (laser)	Fast laser	MRI
EBT2	Green (Good)	Green (Good)	Yellow (Possible)	Yellow (Possible)	Red (Not possible)
nPAG	Red (Not possible)	Red (Not possible)	Green (Good)	Yellow (Possible)	Green (Good)
Presage	Yellow (Possible) / Red (Not possible)	Red (Not possible)	Yellow (Possible)	Yellow (Possible)	Red (Not possible)

Green — Good readout

Yellow — Possible readout after major/minor development

Red — Readout not possible (so far)

The Surrey CCD scanner, developed into a simplified setup called "the flat panel approach", showed great potential for film readout. No gel scanning was performed on the CCD scanner since the internal properties of the irradiated gel make gel scanning very hard. The Presage scan performed with the CCD scanner gave poor result due to an inhomogenous light field, but with a better alignment the readout could be possible.

As both the Octopus IQ and fast laser scanner is categorized as fast laser scanners, they share much of the characteristics and could be stacked together. Film readout was tested with the Octopus scanner and showed some potential. The Octopus was also used to scan a polymer gel dosimeter with good result. A Presage sample was read out using the fast laser scanner and displayed some flaws. For future measurements, more time should be spent on the alignment of the scanner. Furthermore, a larger undistortion test target and a new batch of Presage sample should be used before it is possible to do a fair comparison to other readout methods.

To summarize: All of the optical CT scanners investigated have the potential to be a multi-purpose scanner. However, development is needed in most cases and more measurements have to be carried out to do the thorough investigation needed to reach the answer of the optimal multi-purpose scanner.

6. Acknowledgements

I would like to express my sincere gratitude and deep appreciation to the following people:

- ❖ My supervisors Sofie Ceberg and Sven Bäck for their knowledge, support and encouragement during this project
- ❖ Sven Brink, without whom most of the measurements would not have been possible
- ❖ My foreign collaborators Peter Sandegaard Skyt and Ludvig Muren at Aarhus University and Simon J. Doran and Taufek Abdul Rahman at the University of Surrey, who all welcomed me with open arms
- ❖ And finally everyone that has helped me at the Department of Medical Radiation Physics, SUS Malmö and Lund University. None mentioned, none forgotten

7. References

Adamovics, J. and M. J. Maryanski (2006). "Characterisation of PRESAGE: A new 3-D radiochromic solid polymer dosemeter for ionising radiation." *Radiat Prot Dosimetry* **120**(1-4): 107-112.

Adamovics, J., Maryanski, M.J. (2003). "New 3D Radiochromic Solid Polymer Dosimeter From Leuco Dyes and a Transparent Polymeric Matrix." *Med Phys* **30**(6): 1349.

Amos, W. B. (1991). "Achromatic scanning system." *US Patent* 4997242.

Arjomandy, B., et al. (2010). "Energy dependence and dose response of Gafchromic EBT2 film over a wide range of photon, electron, and proton beam energies." *Med Phys* **37**(5): 1942-1947.

Babic, S. and K. Jordan (2010). Radiochromic Film Densitometry with Vista15 Optical Cone Beam CT Scanner. Poster presented at the 56th Canadian Organization of Medical Physicists (COMP) Annual Meeting, Ottawa, ON, Canada.

Baldock, C., et al. (2010). "Polymer gel dosimetry." *Physics in medicine and biology* **55**(5): R1-63.

Ceberg, S. (2010). "3D Verification of Dynamic and Breathing Adapted Radiotherapy using Polymer Gel Dosimetry". Malmö. PhD thesis, Lund University (ISBN 978-91-7473-041-8).

Ceberg, S., et al. (2010). "RapidArc treatment verification in 3D using polymer gel dosimetry and Monte Carlo simulation." *Physics in medicine and biology* **55**(17): 4885-4898.

De Deene, Y. (2010). "How to scan polymer gels with MRI?" *Journal of Physics: Conference Series* **250**(1): 012015.

De Deene, Y., et al. (2006). "The fundamental radiation properties of normoxic polymer gel dosimeters: a comparison between a methacrylic acid based gel and acrylamide based gels." *Physics in medicine and biology* **51**(3): 653-673.

Devic, S. (2011). "Radiochromic film dosimetry: past, present, and future." *Phys Med* **27**(3): 122-134.

Doran, S. J. (2009a). "The history and principles of chemical dosimetry for 3-D radiation fields: gels, polymers and plastics." *Appl Radiat Isot* **67**(3): 393-398.

Doran, S. J. (2009b). "The history and principles of optical computed tomography for scanning 3-D radiation dosimeters: 2008 update." *Journal of Physics: Conference Series* **164**(1): 012020.

Doran, S. J. (2010). "Imaging and 3-D dosimetry: top tips for MRI and optical CT." *Journal of Physics: Conference Series* **250**(1): 012086.

Ferreira, B. C., et al. (2009). "Evaluation of an Epson flatbed scanner to read Gafchromic EBT films for radiation dosimetry." *Physics in medicine and biology* **54**(4): 1073-1085.

Gore, J. C., et al. (1996). "Radiation dose distributions in three dimensions from tomographic optical density scanning of polymer gels: I. Development of an optical scanner." *Phys Med Biol* **41**(12): 2695-2704.

Hartmann, B., et al. (2010). "Homogeneity of Gafchromic EBT2 film." *Med Phys* **37**(4): 1753-1756.

International Speciality Products (2009). "EBT2 White Paper, Revision 1."

Jordan, K. (2010). "Review of recent advances in radiochromic materials for 3D dosimetry." *Journal of Physics: Conference Series* **250**(1): 012043.

Jordan, K. and J. Battista (2009). "Scatter measurements for optical cone-beam computed tomography." *Journal of Physics: Conference Series* **164**(1): 012028.

Kairn, T., et al. (2010). "Local heterogeneities in early batches of EBT2 film: a suggested solution." *Physics in medicine and biology* **55**(15): L37-42.

Karlsson, A. (2007). "Characterization and clinical application of normoxic polymer gel in radiation therapy dosimetry". Malmö. PhD thesis, Lund University (ISBN 978-91-7473-041-8).

Krstajic, N. and S. J. Doran (2006). "Focusing optics of a parallel beam CCD optical tomography apparatus for 3D radiation gel dosimetry." *Physics in medicine and biology* **51**(8): 2055-2075.

Krstajic, N. and S. J. Doran (2007a). "Characterization of a parallel-beam CCD optical-CT apparatus for 3D radiation dosimetry." *Physics in medicine and biology* **52**(13): 3693-3713.

Krstajic, N. and S. J. Doran (2007b). "Fast laser scanning optical-CT apparatus for 3D radiation dosimetry." *Physics in medicine and biology* **52**(11): N257-263.

Krstajic, N. and S. J. Doran (2009). "Initial characterization of fast laser scanning optical CT apparatus for 3-D dosimetry." *Journal of Physics: Conference Series* **164**(1): 012022.

Lopatiuk-Tirpak, O., et al. (2008). "Performance evaluation of an improved optical computed tomography polymer gel dosimeter system for 3D dose verification of static and dynamic phantom deliveries." *Med Phys* **35**(9): 3847-3859.

McRobbie, D. W. (2007). "MRI from picture to proton", Cambridge, UK. New York. Cambridge University Press (ISBN 9780521865272)

Oldham, M. (2004). "Optical-CT scanning of polymer gels." *J Phys* **3**: 122-135.

Olding, T. and et al. (2009). "Scatter corrections for cone beam optical CT." *Journal of Physics: Conference Series* **164**(1): 012031.

Olding, T., et al. (2010). "Cone beam optical computed tomography for gel dosimetry I: scanner characterization." *Physics in medicine and biology* **55**(10): 2819-2840.

Pawley, J. B. (2006). "Handbook of biological confocal microscopy", New York, NY. Springer.

Sakhalkar, H. S., et al. (2009). "A comprehensive evaluation of the PRESAGE/optical-CT 3D dosimetry system." *Med Phys* **36**(1): 71-82.

Stunja, L., et al. (2010). "A 'quad-phantom' film dosimeter for use as a multi-planar verification tool for PRESAGE/optical-CT." *J Phys* **250**(1): 12097.

The Swedish Cancer Society (2011). "Cancerfondsrapporten 2011".

van Battum, L. J., et al. (2008). "Accurate dosimetry with GafChromic EBT film of a 6 MV photon beam in water: what level is achievable?" *Med Phys* **35**(2): 704-716.

Vergote, K., et al. (2004). "Validation and application of polymer gel dosimetry for the dose verification of an intensity-modulated arc therapy (IMAT) treatment." *Physics in medicine and biology* **49**(2): 287-305.

Wolodzko, J. G., et al. (1999). "CCD imaging for optical tomography of gel radiation dosimeters." *Med Phys* **26**(11): 2508-2513.

Wuu, C. S. and Y. Xu (2006). "Three-dimensional dose verification for intensity modulated radiation therapy using optical CT based polymer gel dosimetry." *Med Phys* **33**(5): 1412-1419.

Zeidan, O. A., et al. (2010). "Dosimetric evaluation of a novel polymer gel dosimeter for proton therapy." *Med Phys* **37**(5): 2145-2152.